
UniMAP
Universiti Malaysia Perlis
Proceedings of
INTERNATIONAL POSTGRADUATE CONFERENCE ON ENGINEERING (IPCE 2010)
Date & Vanue
16th - 17th October 2010
Universiti Malaysia Perlis
(UniMAP)
Perlis, Malaysia
Organised by
Centre for Graduate Studies
Universiti Malaysia Perlis
(UniMAP)
Sponsor:
MOSTI

http://www.allconferences.com/conferences/2010/20100602084738

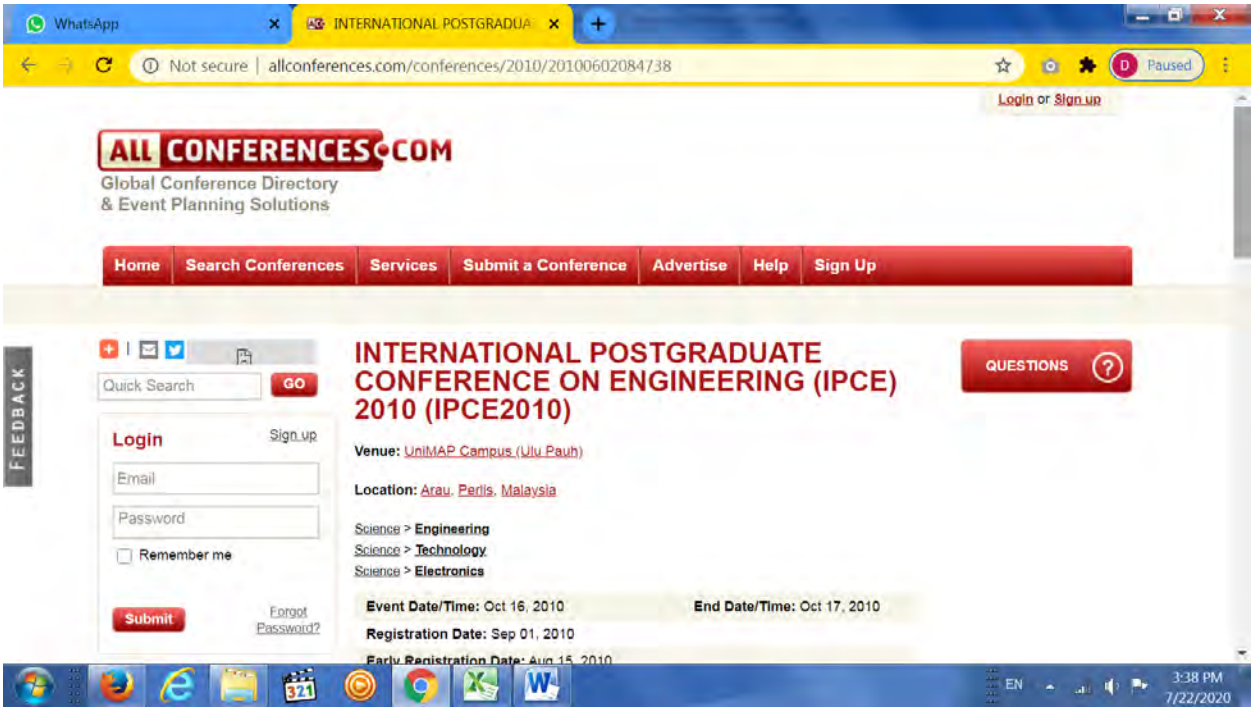

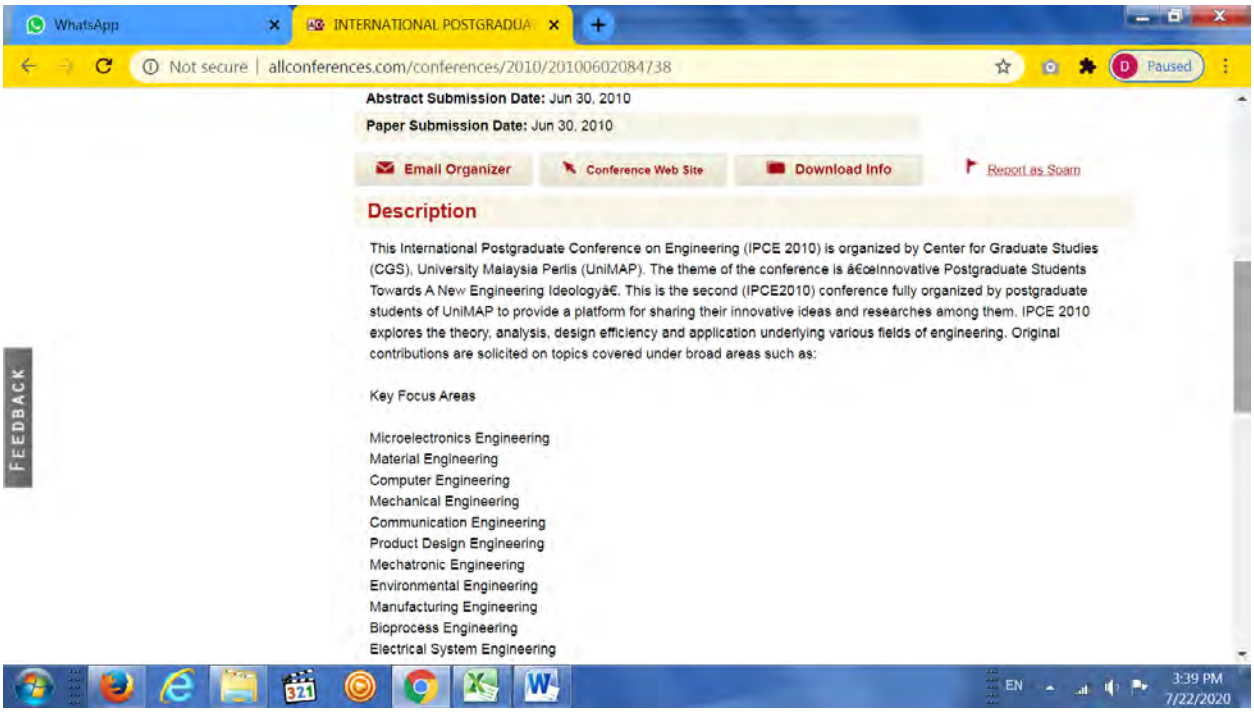

Printed in 2010

ISBN 978-967-5760-03-7

Published by:
Centre for Graduate Studies,
Universiti Malaysia Perlis,
No. 112 & 114 (First Floor), Block A
Taman Pertiwi Indah
Jalan Kangar – Alor Setar, Seriab
01000, Kangar
Perlis, MALAYSIA
Tel: (604) 979 8333, Fax: (604) 979 8334
Email: epcunimap2010@gmail.com

ORGANIZING COMMITTEE

CONFERENCE PATRON

Brigadier General Dato' Professor Dr. Kamarudin bin Hussin

Vice-Chancellor, UniMAP

ADVISORS

Professor Dr Sazali Yaacob

Deputy Vice Chancellor (Academic and International)

Professor Dr Zul Azhar Zahid Jamal

Deputy Vice Chancellor (Research and Innovation)

CHAIRMAN

Professor Dr Mohd Yusoff Mashor

DEPUTY CHAIRMAN I

Bashir Mohammed Ghandi

DEPUTY CHAIRMAN II

Ammar Zakaria

ORGANIZING SECRETARIAT

Norzaililah Zainoddin

Zehan Mat Saad

Annie Sumiyante Mat Isa

Intan Zaheran Azami

Norlizawati Abdullah

Aizat Suhrawady Zainol Abidin

Tengku Khairol Tengku Zabit

CO-CHAIRS

BURSARY	Tan Soo Jin
Sub-committee Members	Elsie Usun Francis Zarimawaty Zailan Nur Syuhada Md. Desa Mohd. Rosydi Zakaria Nurhafizah Ramli Lam Chee Kiang Sim Kwoh Fung
INTERNAL REVIEWS	Bashir Mohammed Ghandi
Sub-committee Members	Muhammed Sabri Erdy Sulino Mohd. Muslim Tan Pubalan A/L Nadaraja Siti Fatimah Abd. Rahman Steven A/L Tanaselas Nur Sheli Akma Ramli Tan Chee Siong Haidar Khalel Qurban Nurul Iwani Alawi Voon Chun Hong Alif Munir Md. Tarmizi
SESSIONS CHAIRMAN	Muthana Yassen Kydir
Sub-committee Members	Ala'eddin Ahmad Jader Saif Iqmal Tahir Thakra S. Dhahi Hayder Khaleel Qurban Ali Faisal Amri Tanjong Thanaa Hussein Abd. Naseer Sabri Salim

PUBLICATION	Muhammad Khusairi Osman
Sub-committee Members	Aimi Salihah Abdul Nasir Norhayati Mohd Nazid Aini Salwa Hasan Nudin Mohd Zubir Suboh Rafikha Aliana A. Raof
PUBLICITY	Nasim Ahmed
Sub-committee Members	Siti Hajar Che Haris
OPENING CAREMONY AND PROTOCOLS	Zainab Nazar Khalil Wafi
Sub-committee Members	Naufal Alee Siti Nasuha Zainal Abidin Mohd Rashidi Che Beson Masita Raja Mohamad Noor Shalasiah Osman
REGISTRATION	Rohadiana Dwi Nofianti
Sub-committee Members	Shaiful Zairi Ahmad Subhi Nor Hazlyna Harun Sri Seskya Situmorang Iqmal Tahir Faisal Amri Tanjong
FOOD AND BEVERAGE	Siti Maryam Sharun
Sub-committee Members	Noor Sara Mashitoh Mohamad Hanif Zul Azfar Ahmam Nurul Hazwani Abdul Halim Norul Nadia Ngah Fatimatul Anis Bakri Muhamad Firdaus Mohamad Dali

ARRANGEMENTS	Mohd Zahiruddin Dzulkifli
Sub-committee Members	Pubalan A/L Nadaraja Allan Melvin A/L Andrew Mohammad Ridhwan Tamjis Azlan Abd. Ghani Zamzamir Said
ACCOMODATION	Ammar Zakaria
Sub-committee Members	Latifah Munirah Kamarudin Muhd. Ezanuddin Abd. Aziz Nor Muzakkir Nor Ayob Wee Fwen Hoon

C) Electrical System Engineering

http://103.86.130.60/handle/123456789/21224

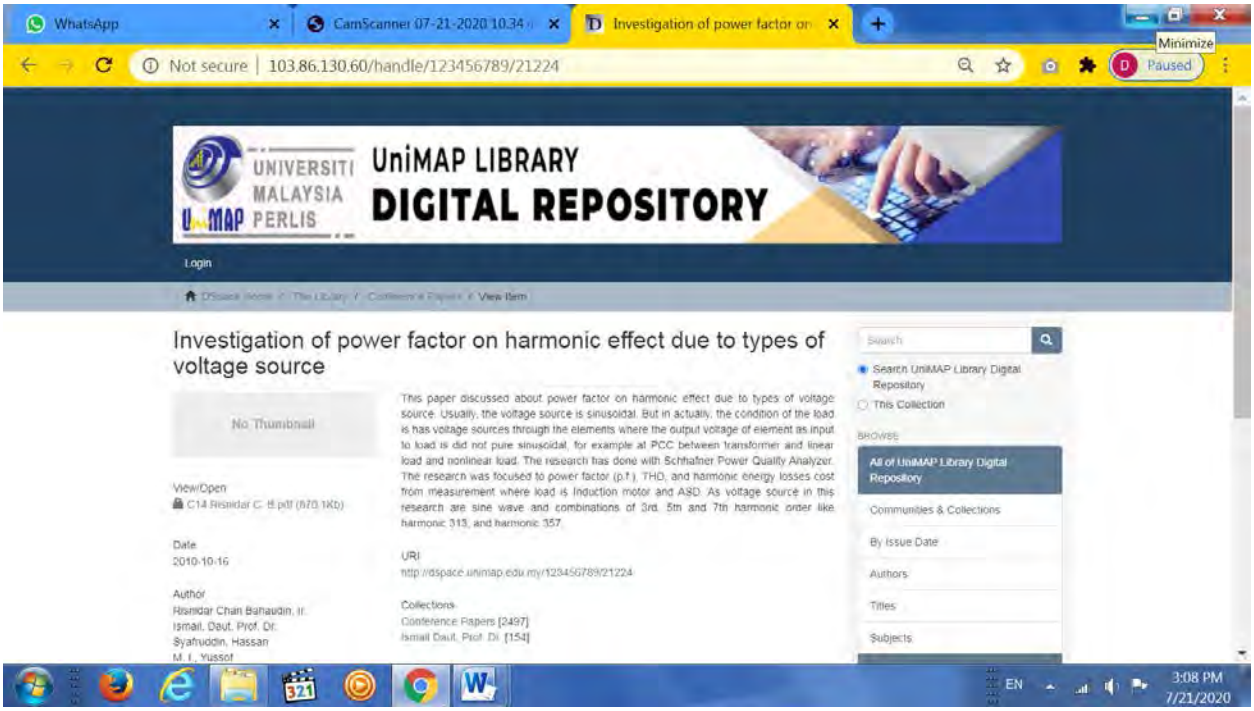

Proceedings of the International Postgraduate Conference on Engineering (IPCE 2010)
16 - 17 October 2010, Perlis, Malaysia

Investigation of Power Factor on Harmonic Effect due to Types of Voltage Source

[1]Risnidar C.B, [2]Ismail Daut,.[1]Syafruddin H.S. [1]M.I. Yussof, [1]Rosnazri A,
[1]Dina M.M. Ahmad, [3]Masykur, [4]Indra N
[1]Ph.D student UniMAP, [2]Supervisor Ph.D student UniMAP
Electrical Engineering Department, University Malaysia Perlis (UniMAP), Kangar, Malaysia
[3]Master Student USU
Electrical Engineering Department, Universitas Sumatera Utara, Medan, Indonesia.
[4]Ph.D student USM
Electrical Engineering Department, University Science Malaysia, Malaysia
Email: risnidar@unimap.edu.my

Abstract

This paper discussed about power factor on harmonic effect due to types of voltage source. Usually, the voltage source is sinusoidal. But in actually, the condition of the load is has voltage sources through the elements where the output voltage of element as input to load is did not pure sinusoidal, for example at PCC between transformer and linear load and nonlinear load. The research has done with Schhafner Power Quality Analyzer. The research was focused to power factor (p.f), THD, and harmonic energy losses cost from measurement where load is Induction motor and ASD. As voltage source in this research are sine wave and combinations of 3rd, 5th and 7th harmonic order like harmonic 313, and harmonic 357.

Keywords—type of voltage source, power factor, energy losses cost, harmonic, THD.

1. Introduction

Caused in this research discussing the kinds of voltage sources used to serve the load, such as sine wave, square wave and the combination of the harmonics order, so necessary to discuss about Fourier series. Because to analyze the harmonics, applied the Fourier series is appropriate. Actually, Fourier series is a periodic function can be written as sums of infinitely many sine and cosine functions of different frequencies [1] R.J. Beerends et al (2003), often expressed in terms of the angular frequency. Harmonic waveform distortion is one of the most important issues today. In this paper discuss about investigation of harmonic effect due to harmonic types of voltage source, where voltage sources are a few types of harmonic waveform. This case is as a part of system, where if a Point of Common Coupling (PCC) of one component nonlinear load has supplied with another nonlinear load. In this research, the load is Induction Motor with ASD was supplied with Sine waveform, Harmonic 3rd, 5th, and 7th combination waveform.

The presence of harmonic distortion in the applied voltage to a motor will both increase electrical losses and decrease efficiency. These losses will increase motor temperature, resulting in even further losses These currents passing through the system impedance cause voltage drops for each individual harmonic, resulting in distortion of the voltage's waveform. The effect of harmonic distortion of the voltage waveform due to impacts motor performance as p.f. IHD and THD for current and voltage, and energy losses due to harmonic. [2][3][4].

One of main harmonics characteristic is: p.f. This is a measure of how effectively a specific load consumes electricity to produce work. The higher of power factor, the more work produced for a given voltage and current. The relationships between power vector to explain about power factor as Figure 1. From Figure 1, the relationship between power and power factor for Linear Loads and Non-Linear Loads are as follow.

a. Linear Loads

$$p.f. = \frac{P}{S} = \frac{kW}{kVA} = \cos\varphi \qquad (1)$$

ISBN 978-967-5760-03-7

$$S = \sqrt{P^2 + Q^2} \quad (2)$$

$$kVA = \sqrt{kW^2 + kVAR^2} \quad (3)$$

b. Non-Linear Loads

$$p.f = \frac{P}{S} = \frac{kW}{kVA} = \cos\varphi \quad (4)$$

$$S = \sqrt{P^2 + Q^2} \quad (5)$$

$$kVA = \sqrt{kW^2 + kVAR^2 + kVAR_H^2} \quad (6)$$

True Power factor = (Displacement p.f) x (Distortion p.f)

The others characteristic of harmonic are:

The values of V_{rms} I_{rms}, Power (P), were calculated directly from the harmonic components obtained with a Fast Fourier Transform of the sampled data of the voltage and current waveforms of the Induction Motor under tests. These quantities were calculated as:[3][4][5][6]

$$V_{rms} = \sqrt{\sum_{h=1}^{\infty} V_h^2} \text{ and } I_{rms} = \sqrt{\sum_{h=1}^{\infty} I_h^2} \quad (7)$$

$$P = \sum_{h=1}^{\infty} V_h I_h \cos\varphi_h \text{ and } S = V_{rms} I_{rms} \quad (8)$$

where V_h, I_h φ_h are magnitudes and phase shift of the voltage and current, h order harmonic.

The factor that measures the distortion in the non sinusoidal wave is Total Harmonic Distortion (THD) where this factor is defined for both voltage and current as below:

$$THD_I = \frac{\sqrt{\sum_{h=2}^{\infty} I_h^2}}{I_1} \text{ and } THD_V = \frac{\sqrt{\sum_{h=2}^{\infty} V_h^2}}{V_1}$$

2. Methodology

From the measurement of induction motor with Shaffner, where the voltage source to load is varieties are: sinusoidal, and a few harmonics waveforms. And the load is three phase induction motor. These experiments are done, because to investigated the effect of voltage source type of harmonic to served load. Because at any PCC in power system, the load maybe find source did not pure sinusoidal, for example from secondary of transformer. The main characteristic of harmonics are Individual Harmonic Distortion (IHD) for 3rd ,5th and 7th, Tota. Harmonic Distortion (THD) for voltage and current, Power losses due to harmonics, power factor, Cress factor for each harmonics, I_{rms}, V_{rms}. The measurements are done with voltage sources variable from 160 V until 240 V.

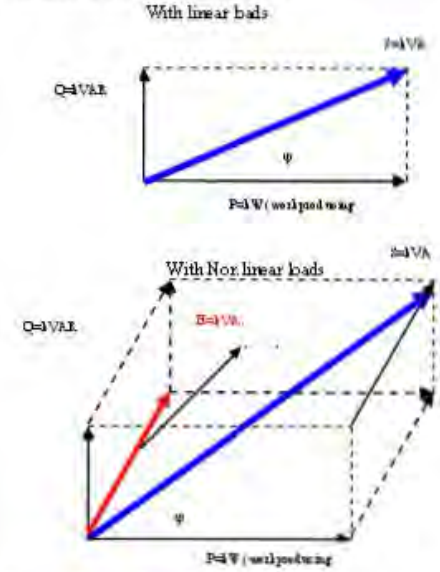

Figure1. Power factor relationship for Linear and Non-Linear loads

Figure2. Type of voltage source from 3rd, 5th and 7th Harmonic order combinations

Figure3. Induction Motor Measurement

The type of voltage source from combination of harmonic order 3rd, 5th and 7th are as Figure 2:

The Induction motor specifications are: 3 phase, 1.5 Hp, 50 Hz, 1370 rpm, 4 poles. The measurements have done with ASD.

3. Data and result

Data and result base direct measurements to Induction motor 3 phase, 1.5 Hp, 50 Hz, 1370 rpm, 4 poles are as follow:

Table1. Type of voltage source Vs, real power at phase A, B and C.

No	Voltage source	Phase A	Phase B	Phase C
1	Harm313	0.057	0.075	0.020
2	Harm357	0.041	0.060	0.024
3	Sine	0.037	0.069	0.033
4	Square	0.034	0.031	0.016

Table2. Type of voltage source Vs apparent power at phase A, B and C

No	Voltage source	Phase A	Phase B	Phase C
1	Harm313	0.216	0.234	0.097
2	Harm357	0.152	0.180	0.100
3	Sine	0.127	0.176	0.122
4	Square	0.117	0.120	0.068

Table3. Type of voltage source Vs power factor (p.f.) at phase A, B and C

No	Voltage source	Phase A	Phase B	Phase C
1	Harm313	0.27	0.32	0.21
2	Harm357	0.27	0.34	0.24
3	Sine	0.29	0.39	0.27
4	Square	0.29	0.26	0.25

Table4. Type of voltage source Vs Cress Factor (C.F.) at phase A, B and C

No	Voltage source	Phase A	Phase B	Phase C
1	Harm 313	8.33	7.71	8.43
2	Harm 357	7.42	6.25	7.34
3	Sine	7.57	5.21	6.72
4	Square	6.03	5.94	6.71

Table5. Type of voltage source Vs THD voltage harmonic at phase A, B and C

No	Voltage source	Phase A	Phase B	Phase C
1	Harm 313	9.91	9.83	9.88
2	Harm 357	13.12	13.09	13.09
3	Sine	0.27	0.27	0.23
4	Square	41.11	41.07	41.10

Table6. Type of voltage source Vs THD current harmonic at phase A, B and C

No	Voltage source	Phase A	Phase B	Phase C
1	Harm313	94.67	92.78	
2	Harm357	92.40	90.24	
3	Sine	91.20	87.33	
4	Square		84.70	

The voltage and current characteristics of each voltage source type are as in Figure 4 below

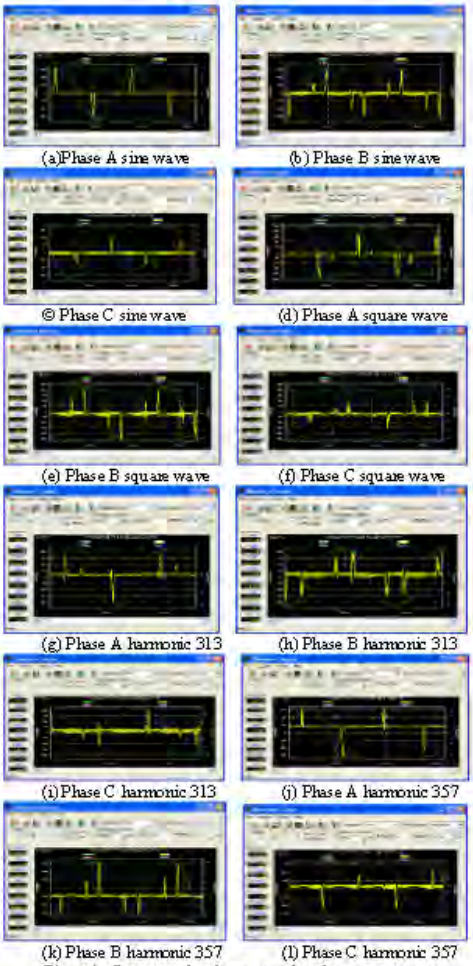

(a)Phase A sine wave (b) Phase B sine wave
© Phase C sine wave (d) Phase A square wave
(e) Phase B square wave (f) Phase C square wave
(g) Phase A harmonic 313 (h) Phase B harmonic 313
(i) Phase C harmonic 313 (j) Phase A harmonic 357
(k) Phase B harmonic 357 (l) Phase C harmonic 357

Figure4. Current and voltage at each voltage source type

4. Analysis

From experiment data and results the analysis for harmonic characteristics are as follow:

4.1. Real power (P) in kW

For real power P, harmonic 313 is highest (0.057) phase A, (0.075) phase B, but for phase C is sine wave (0.033). The smallest is square wave (0.034), phase A, (0.031) phase B and (0.016) phase C.

4.2. Apparent power (S) in kVA

The highest apparent power is harmonic 313 (0.216) phase A, (0.234) phase B but for phase C, sine wave (0.122). The lowest is square (0.117) phase A, (0.120) phase b and (0.068) phase C.

4.3. Power factor (p.f.)

Power factor (p.f) for sine wave is highest in all phase (0.29), (0,39) and (0.27) and square wave is highest (0.29), while the others voltage source just the same (0.27) in phase A, but in phase B square wave is lowest and in phase c harmonic 313 is lowest (0.21)

4.4. Cress Factor (C.F.)

For Cress Factor (C.F.) square wave is smallest in phase A (6.03), and C (6.71) while harmonic 313 is highest in all phase (8.33), (7.71) and (8.43.

4.5. THD voltage harmonic

For voltage Total Harmonic Distortion (THD) Sine wave is the smallest for all phase (0.27%), (0.23%), while square wave is the biggest (41.11%), (41.07%) and (41.10%).

4.6. THD current harmonic

For current Total Harmonic Distortion (THD) harmonic 313 is biggest (94.67%) and (92.78), while the smallest is square wave (90.21%) and (84.70)

5. Conclusion

From analyze, the conclusion are:

1. Real power and apparent power loss due to type of voltage source, harmonic 313 is biggest.
2. Power factor (p.f.) for sine wave is highest in all phase and square wave also, while the others voltage source just the same in phase A, but in phase B square wave is lowest and in phase c harmonic 313 is lowest
3. For Cress Factor (C.F.) square wave is smallest in phase A and C while harmonic 313 is highest in all phase
4. For voltage Total Harmonic Distortion (THD) Sine wave is the smallest for all phase, while square wave is the biggest.
5. For current Total Harmonic Distortion (THD) harmonic 313 is biggest, while the smallest is square wave.

6. Acknowledgement

The authors would like to express their gratitude to the Fundamental Research Grant Scheme (FRGS), School of Electrical System Engineering of Universiti Malaysia Perlis (UniMAP) and Power Electronics and Electrical Machine Design Research Cluster for the supply of research facility respectively.

7. References

[1]. R. J. Beerends, H. G. Morshe, J. C. van den Berg and E. M. van de Vrie, "*Fourier and Laplace Transforms*", Translated from Dutch by R.. J. Beerends, Cambridge University Press, 2003.

[2]. Peter Bechard, *"Fault ZoneAnalysis POWER QUALITY"*, The 2004 Motor Reliability Technical Conference, PdMA Corporation.

[3]. Barry W. Kennedy, POWER QUALITY PRIMER, McGraw-Hill, Singapore, 2000

[4]. Francisco C. De La Rosa, "Harmonics and Power Systems", Taylor & Frencis, CRC, Boca Raton, 2006.

[5]. J. Arrilaga, B.C.Smith, N.R. Watson, A.R. Wood, POWER SYSTEM HARMONIC ANALYSIS, John Wiley & Sons, Singapore, 2000

[6]. IEEE Recommended Practices and Requirements for Harmonic Control in Electrical Power Systems

http://103.86.130.60/handle/123456789/21301

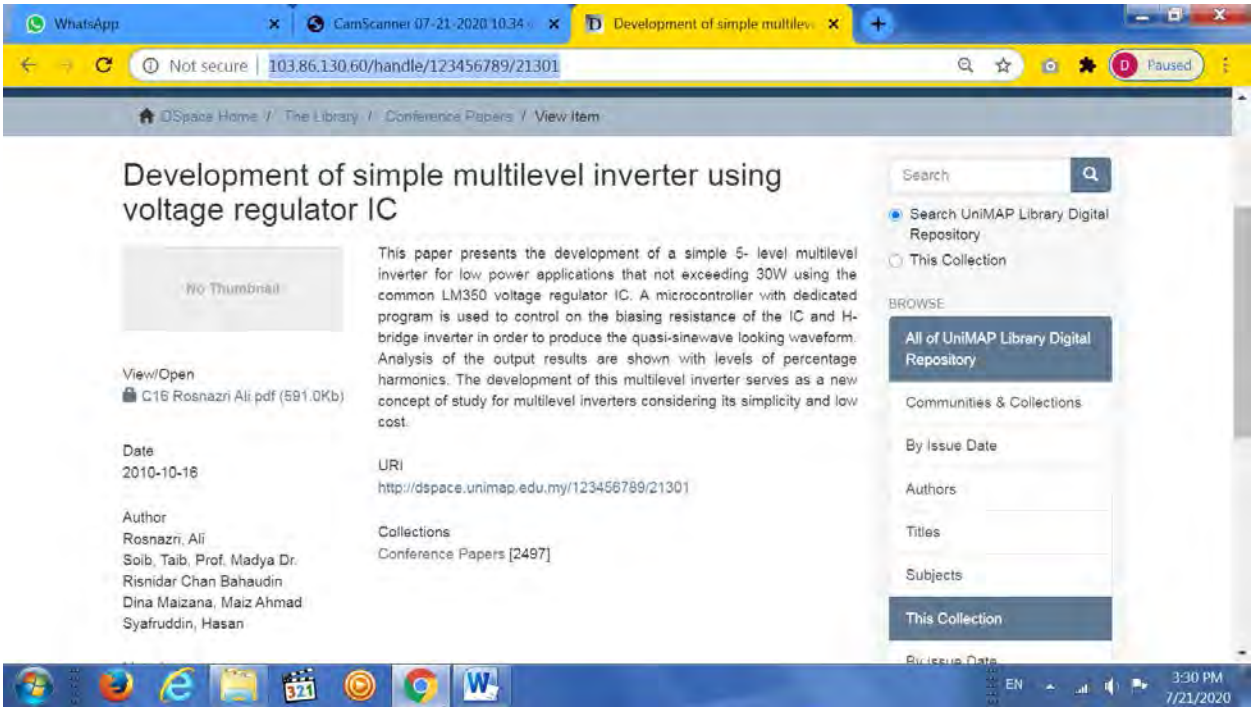

Proceedings of the International Postgraduate Conference on Engineering (IPCE 2010)
16 - 17 October 2010, Perlis, Malaysia

Development of Simple Multilevel Inverter Using Voltage Regulator IC

Rosnazri Ali[1], Ismail Daut[1], Soib Taib[2], Risnidar C.B[1], Dina M.M. Ahmad[1], Syafruddin Hasan[1]

[1]*School of Electrical Systems Engineering,*
Universiti Malaysia Perlis.
E-mail: rosnazri@unimap.edu.my

[2] *School of Electrical & Electronic Engineering,*
Universiti Sains Malaysia.
E-mail: soibtaib@eng.usm.my

Abstract

This paper presents the development of a simple 5-level multilevel inverter for low power applications that not exceeding 30W using the common LM350 voltage regulator IC. A microcontroller with dedicated program is used to control on the biasing resistance of the IC and H-bridge inverter in order to produce the quasi-sinewave looking waveform. Analysis of the output results are shown with levels of percentage harmonics. The development of this multilevel inverter serves as a new concept of study for multilevel inverters considering its simplicity and low cost.

1. Introduction

Multilevel inverters have drawn significant interest in the power industry both in the industrial electronics and renewable energy applications. Such power converters that invert DC to AC have been the prime focus of many power electronic researches in order to produce high performance, reliable, energy efficient at minimum cost. Ideally, an inverter is supposed to produce a perfect sinusoidal voltage waveform from a DC source, suitable to power-up common AC appliances without any operational problems.

The inherent advantages of multilevel inverters are having lower harmonics output, lower EMI generation, better output waveform (closer to sinusoidal), lower device voltage stress and higher efficiency. With more level, the staircase waveform is much closer to the sinusoidal waveform [1][2]. Conversely, the disadvantages of multilevel inverters are too overwhelming. The complexity of their circuits, involving many DC supply sources, switching components, capacitors, complicated modulations and switching techniques, have made the multilevel inverters technically challenging and costly [3][4].

In this paper, simple novel approach of producing a 5-level multilevel inverter for low power applications using a voltage regulator IC (LM350) is introduced. In reference to its data sheet [5], the typical guaranteed output current (I_o) to a load is 3A with variable output voltage (V_o) from 1.2V to 33V and the differential input and output voltage ($V_i - V_o$) is in between 3V and 35V. Series biasing resistors are connected to the adjustment terminal of the IC regulator to get different output voltages as the selection of the resistors is controlled by a microcontroller (PIC16F628). A program was written into the microcontroller to turn-on and off respective resistors in correct sequence and control the MOSFETs of the bridge inverter in order to get the multilevel output voltage closer to sinusoidal waveform. Depending on the program, the inverter can be made to generate 50 Hz, 60Hz or other desirable frequency waveforms at the output.

2. Methodology

The block diagram of the concept is as shown in Figure 1. The voltage regulator IC with biasing resistors is represented as the Programmable Adjustable Voltage Regulator block.

ISBN 978-967-5760-03-7

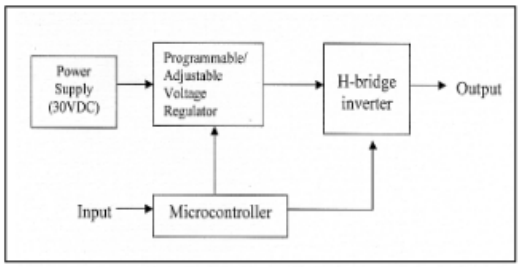

Figure 1. Concept of the multilevel inverter

2.1. Design components of the voltage regulator

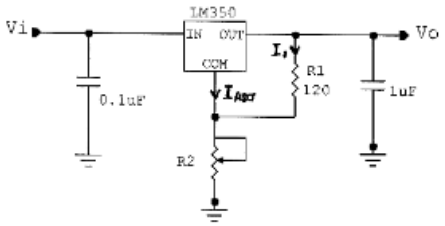

Figure 2. Typical application of LM350

Referring to the Figure 2, the output voltage (V_o) is determined by,

$$V_o = 1.25V(1+\frac{R_2}{R_1}) + I_{ADJ}R_2 \qquad (1)$$

where R_1 and R_2 are the biasing resistors and I_{ADJ} is the adjustment terminal current which is normally less than 100uA.
For simplicity, an empirical formula is used to get the output voltage as required. R_1 is chosen to be 120 Ω.

$$V_o = \frac{R_2 + 120}{96} \qquad (2)$$

Let's consider that R_2 consists of 4 identical resistors R_a, R_b, R_c, R_d with small signal transistors (T1, T2, T3 & T4) connected across them as indicated in Figure 3. The purpose of the transistors is to switch the biasing resistors in sequence in order to generate 4 different voltage levels to the output. By applying formula (2) and consider that $R_a = R_b = R_c = R_d = 560\ \Omega$, then the output voltages (V_o) are shown in Table 1.

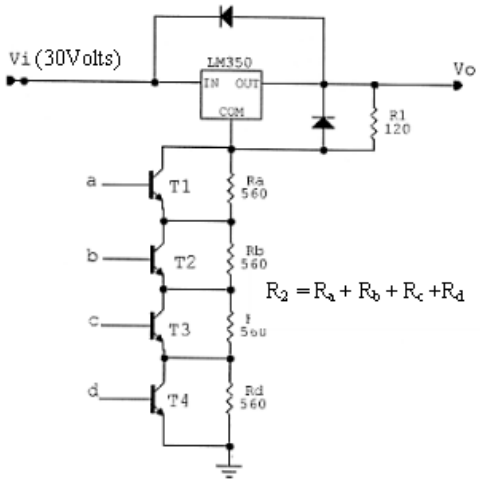

Figure 3. LM350 circuit with switching transistors

Table 1. Selection of output voltages (Vo)

Logic				Total R2 (Ohms)	Vo (Volts)
a	b	c	d		
1	1	1	1	0	1.31
0	1	1	1	560	7.15
0	0	1	1	1120	12.90
0	0	0	1	1680	18.75
0	0	0	0	2240	24.58

Logic 0 - Low (0V)
Logic 1 - High (+5V)

By applying logic signals to the base of transistors T1 ~ T4, the total resistance R_2 that acts as the biasing resistant to the voltage regulator IC will change its value accordingly. Hence generating different output voltages (V_o) whereby providing direct supply to an H-bridge inverter.

2.2. Microcontroller and H-Bridge Inverter Circuit

To generate the necessary logic signals and sequential controls for the voltage regulator IC and H-bridge inverter, a microcontroller PIC16F628 is used as the main controller. Figure 4 shows the diagram of the circuit.

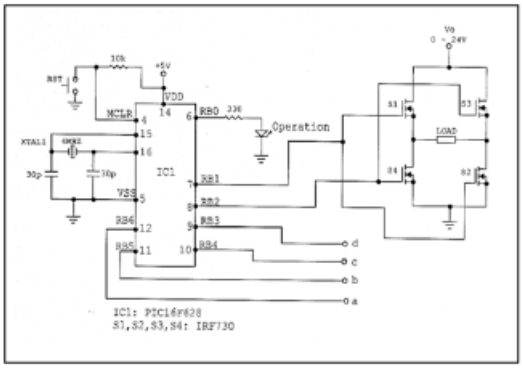

Figure 4. Microcontroller and bridge inverter circuit

2.3. Determination of switching intervals for a 50Hz sinewave

Consider the full sinewave equation (3) as given,

$$v(t) = V_m \sin \omega t \qquad (3)$$

where $v(t)$ is the instantaneous voltage, V_m is the peak amplitude and $\omega = 2\pi f$. In this case, $f = 50Hz$, $V_m = 24v$ and $v(t) = V_o$.

Using equation (3), the timing parameters of voltage control levels to create a sinewave is tabulated as in Table 2.

Table 2. Voltage and timing controls

(Volts)	Milliseconds										
Vo	t0	t1	t2	t3	t4	t5	t6	t7	t8	t9	t10
1.31	0.000										10.000
7.15		0.963								9.037	
12.90			1.806						8.194		
18.75				2.854				7.146			
23.50*					4.349		5.651				
24.00						5.000					

* In order to create a flat top waveform at the peak, the maximum voltage (Vo) is assumed to be 23.5V and taken into the equation to get t4 and t6.

For further details, Figure 5 simplifies the timing sequence and voltage controls of Table 2 into a visualize form.

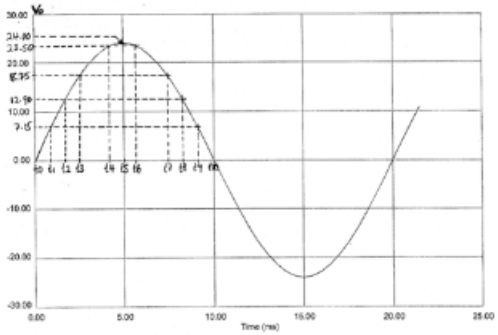

Figure 5. Half-cycle of the sinewave voltage and timing controls

2.4. Flowchart of the program control software

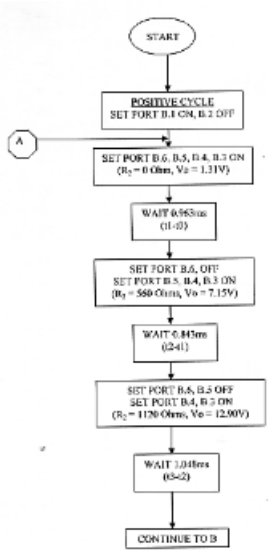

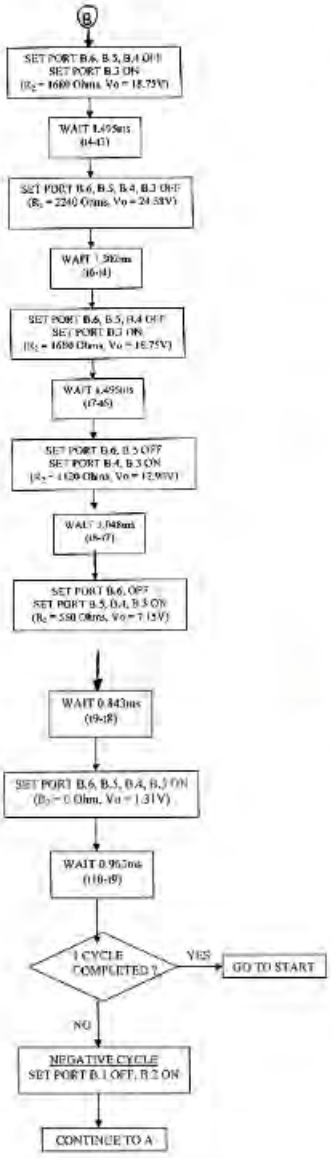

Figure 6. Flowchart of the program

As shown in Figure 6, the program control software was written into the microcontroller to control the output ports assigned as Port B.0 until B.6. The program is in closed loop condition, in such that the program will run continuously producing the quasi-sine waveform with complete positive and negative cycles.

3. Results

The multilevel inverter circuit using voltage regulator IC was assembled into proto-boards as shown in Figure 7. Excessive heat is expected to develop across the voltage regulator IC due to the potential difference of Vo and Vi, especially when the load current is around 1A. Therefore, an appropriate sizing of heat sink should be installed to ensure adequate heat dissipation out of the IC so that the IC temperature is within its operating region.

Figure 7. View of the prototype assembled into a box

Figure 8 shows the output voltage waveform of the multilevel inverter as displayed through an oscilloscope. It can be seen clearly the 5-step voltages that forming the waveform and the output is approximately similar to a sinewave.

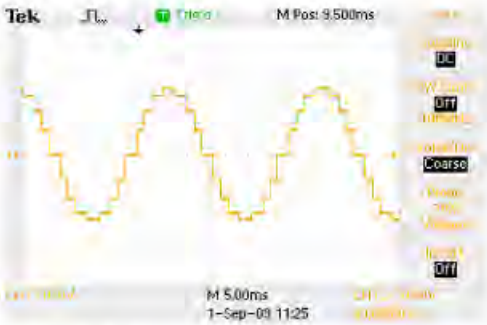

Figure 8. Output voltage waveform of the inverter

Analysis of the output waveform was taken using a power analyzer PM100 and the results are tabulated in Table 3. All even harmonic values were too small and insignificant to be taken into account.

Vo = 13.84 Vrms
Voltage THD = 10.81%
1st Harmonic (fundamental) Voltage = 13.762 Vrms

Table 3. Harmonic numbers and percentage harmonics

Harmonic No.	3	5	7	9	11	13
%	0.568	3.871	3.561	1.614	3.864	1.284

The harmonics spectrum of the output waveform is then plotted as depicted in Figure 9 below.

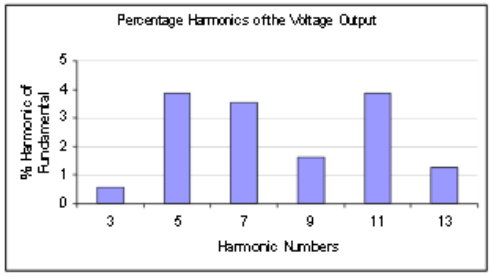

Figure 9. Harmonics spectrum of the output waveform

It is observed that all of the harmonic numbers percentage is under 4% percent of the fundamental, in which tolerable in most cases.

4. Conclusion

A 5-level multilevel inverter using a voltage regulator IC (LM350) has been proposed and tested. It was shown that the method of controlling biasing resistance of the adjust terminal of the regulator IC will produce different voltage levels. A microcontroller is used to fully control on the inverter operation as to produce the necessary output voltage waveform.
For better harmonics elimination, smoothing inductor and capacitor can be connected across the output of the inverter to further eliminate or reduce the step voltages, thus will improve the harmonic contents and waveform to look as a pure sinewave.

Future exploration in the concept can be made in parallel-up few of the voltage regulator ICs so that increasing the output current for heavier load. Further more, a step-up transformer can also be connected to the low-voltage output to increase the voltage to run common AC electrical appliances.

5. References

[1] Ahmad, M.I.; Husin, Z.; Ahmad, R.B.; Rahim, H.A.; Abu Hassan, M.S.; Md Isa, M.N.; , "FPGA based control IC for multilevel inverter," *Computer and Communication Engineering, 2008. ICCCE 2008. International Conference on* , vol., no., pp.319-322, 13-15 May 2008

[2] Alian Chen; Chenghui Zhang; Hao Ma; Yan Deng; , "A novel multilevel inverter topology with no clamping diodes and flying capacitors," *Industrial Electronics, 2008. IECON 2008. 34th Annual Conference of IEEE* , vol., no., pp.3184-3187, 10-13 Nov. 2008

[3] Ceglia, G.; Grau, V.; Guzman, V.; Sanchez, C.; Ibanez, F.; Walter, J.; Millan, A.; Gimenez, M.I.; , "A new multilevel inverter topology," *Devices, Circuits and Systems, 2004. Proceedings of the Fifth IEEE International Caracas Conference on* , vol.1, no., pp. 212- 218, 3-5 Nov. 2004

[4] Khomfoi, S.; Aimsaard, C.; , "A 5-level cascaded hybrid multilevel inverter for interfacing with renewable energy resources," *Electrical Engineering/Electronics, Computer, Telecommunications and Information Technology, 2009. ECTI-CON 2009. 6th International Conference on* , vol.01, no., pp.284-287, 6-9 May 2009

[5] http://www.fairchildsemi.com/ds/LM/LM350.pdf

http://103.86.130.60/handle/123456789/21309

Proceedings of the International Postgraduate Conference on Engineering (IPCE 2010)
16 - 17 October 2010, Perlis, Malaysia

Flux Pattern in 1000 kVA 11/.433 kV Distribution Transformer Core To Sinusoidal Wave

Shahanom Uthman, Ismail Daut, Dina M.M.
shah@mtm.com.my, ismail.daut@unimap.edu.my dina@unimap.edu.my

Abstract

A study was conducted using sinusoidal waveform to capture flux pattern in CRGO M5 material in a 1000kVA 11kV 3 phase transformer core. It is found that it takes about 180° electrical degree cycle for a pool of flux to migrate from one core limb to the other two limb. The computed and experimental values at 1.7T flux density for the core losses had shown a difference of 4.2 %. There are two loops of flux flow exist at any phase(ωt) angle in the core. The hotspot area of the core is near the inner core of the T joint and along the core window. The 2D FEM software used has satisfied and fulfill the objective of the work interest.

1. Introduction

The aim of presenting this paper is to provide contribution to the understanding of transformer losses and its flux pattern behavior with regard to the excitation current in each core limb. A 2D finite element method software is used to assist the simulation of the flux pattern in the core. Actual values for the excitation currents are used from the experiment done on the core. There are numerous research works that had been carried out to understand the behavior of flux and its criteria contribute to core losses.[1,2,3] The behavior of flux flow in the core is important to the transformer designers in order to achieve optimum performance of the transformer.

2. Methodology

The work method that is applied under this experiment work is done as follows:

1) A transformer core with 45° V notch off set design is selected for this work as shown in Figure 1 (a).

2) The test circuit for the experiment is displayed in Figure 2. Each core limb will have the 200 turn for primary and secondary winding connected in Y configuration. The experiment is executed at induction level from 1T to 2 T and current excitation in each core limb and the losses values are recorded accordingly.

3) For the simulation work using 2D FEM, need to insert the BH material values, anisotropy values from DC magnetization curve at 45° and current excitation values in 2) corresponding to sinusoidal angle ωt as per Figure 3.

4) Perform simulation with FEM software

5) Analyze flux pattern and compare loss values between computational and actual laboratory work

The core losses and flux pattern study was performed on a 1000 kVA 11/.433 kV to TNB specification. A core design using V notch core design with 45° center limb cutting were tested under this work. The grade of CRGO material used in the transformer core is M5. The core design is shown in Figure 1. The core is assembled with a 10 layer thickness as per Figure 1(b) The V-notch T joint geometrical design is having 7.1 mm peak to peak distance with 5mm overlap gap. The corner joint is using normal 45° mitred cut.

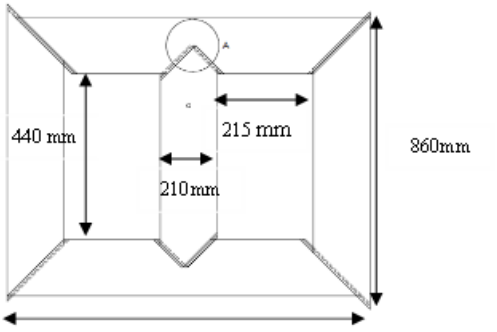

Figure 1 (a)

ISBN 978-967-5760-03-7

Figure 1(b)

Test circuit for no load loss is following IEC 60076 requirement under transformer routine test standard using three watt meter method.

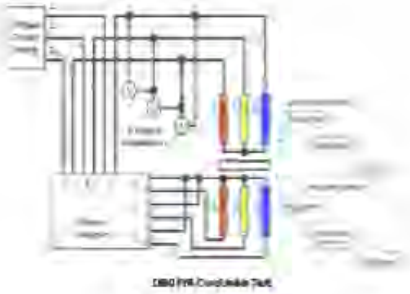

Figure 2

All equipment used during the experiments are calibrated to within ± 5% accuracy values. The flux induction values from 1T to 2T and the core losses are recorded accordingly.

The FEM software used in this work is called Finite Element Method Magnetics (FEMM) version 4.2 developed by David Meeker of USA. Over the years the software have been evolving with improvements and it is given free from the internet to any interested party who like to pursue study on electromagnetic analysis work. For magnetostatic fields, FEMM solves Maxwell's equation that can be considered as 'low frequency problems' in which displacement current can be ignored.

Magnetostatics problems are problems in which the fields are time-invariant. In this case, the field intensity (H) and flux density (B) must obey.

$$\nabla \times B = J \qquad (1)$$

$$\nabla \cdot B = 0 \qquad (2)$$

$$B = \mu H \qquad (3)$$

Should a material is a nonlinear, the permeability, μ is actually a function of B such as

$$\mu = \frac{B}{H(B)} \qquad (4)$$

FEMM software satisfies equation (1) to (3) via a magnetic vector potential known as A to solve

$$B = \nabla \times A \qquad (5)$$

Definition B always satisfies equation (2) and equation (1) can be rewritten as

$$\nabla \times \left[\frac{1}{\mu(B)} \nabla \times A \right] = J \qquad (6)$$

FEMM uses equation (6) to solve magnetostatic problems that involves nonlinear B-H relationship. [4]

The advantage of using the vector potential formulation is that all the conditions to be satisfied have been combined into a single equation. If A is found, B and H can be deduced by differentiating A.

3. Result and Discussion

The experiment test result for the full induction level up to 2T is shown in Table 1.

Voltage	B	Ploss
V	T	W
26.85	1T	6.409
29.54	1.1T	8.33
32.22	1.2T	9.406
34.91	1.3T	10.918
37.59	1.4T	12.654
40.28	1.5T	14.425
42.96	1.6T	16.351
45.65	1.7T	18.858
48.33	1.8T	21.31
51.01	1.9T	23.7
53.7	2T	25.44

Table 1

The actual excitation current in the 3 core limb will be fed into a sinusoidal graph in order to get the ωt angle as shown in Figure 3.

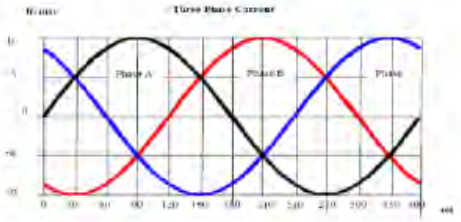

Figure 3

The 3 phase current in the core limb at 1.7T induction is displayed in Table 2.

	Angle												
Phase	0	30	60	90	120	150	180	210	240	270	300	330	360
A-max.g	0.500	0.559	0.852	1.000	0.852	0.559	0.500	-0.500	-0.852	-1.000	-0.852	-0.500	0.500
B-max.g	-0.852	-1.000	-0.852	-0.559	0.500	0.559	0.852	1.000	0.852	0.559	0.500	-0.852	-0.852
C-max.g	0.852	0.559	0.500	-0.559	-0.852	-1.000	-0.559	-0.500	0.500	0.559	0.852	1.000	0.852

Table 2

The construction of the core model in the FEMM mode is shown in Figure 4.

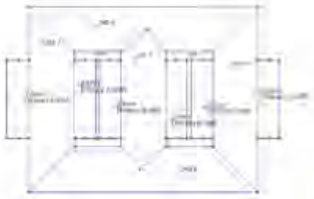

Figure 4

To take the anisotropic effect of the core the permeability in x direction μ_x particularly in the yoke is superior than in y direction. Likewise, in the core limb the permeability μ_y is superior than x direction in the core end limb and center limb. The value of the permeability in either x or y direction magnetization can be captured from the DC magnetization curve given by the CRGO manufacturer.[5]

From the excitation current information in Table 2 the values of the current with the corresponding core limb and angular displacement angle ωt is fed into the FEMM software and the result for the flux pattern is shown in Figure 5a to 5g. Since the flow of the flux is following symmetrical trend, the pattern will be shown up to half cycle.

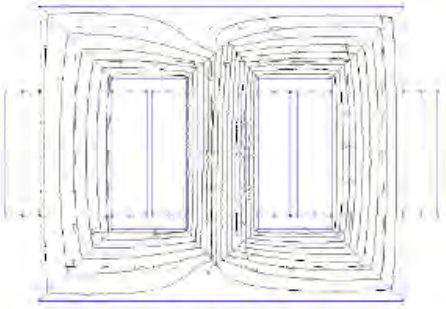

Figure 5(a) ωt = 0

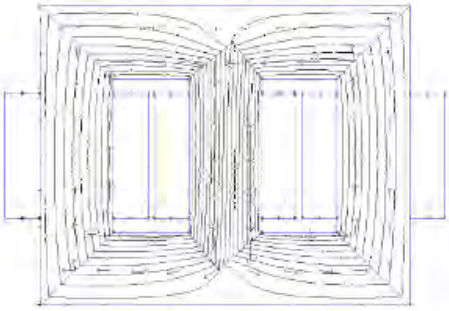

Figure 5(b) ωt = 30

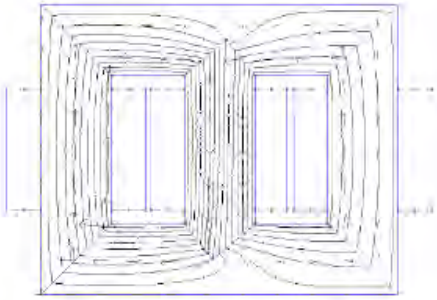

Figure 5(c) ωt = 60

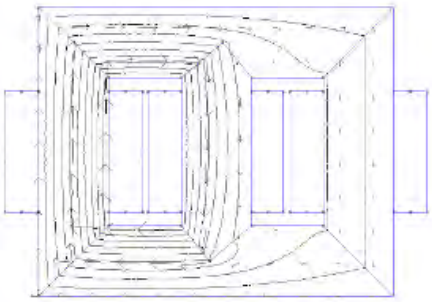

Figure 5(d) ωt = 90

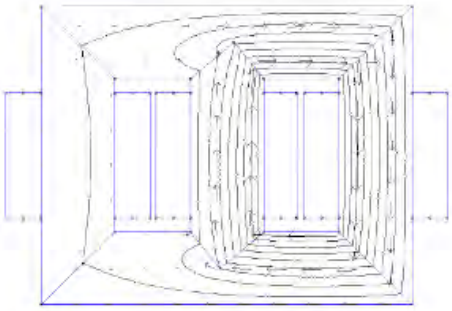

Figure 5(g) ωt = 180

From the observation of the flux lines one can notice that the equipotential lines run along the rolling direction toward the corner joints as well as the T joint in the middle of the core have a definite embedded nature of anisotropy material.

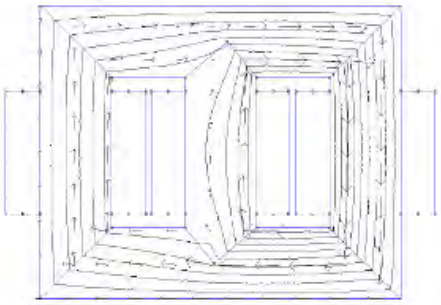

Figure 5(e) ωt = 120

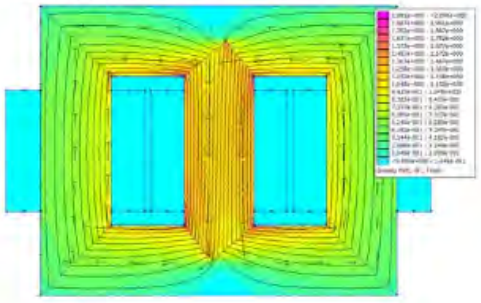

Figure 6 (a)

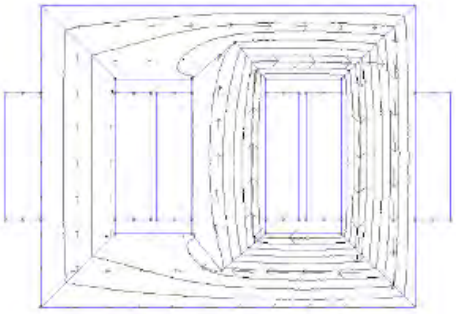

Figure 5(f) ωt = 150

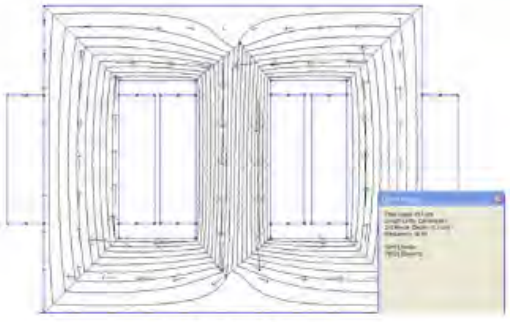

Figure 6 (b)

The overall core loss by experiment work at 1.7 T induction is recorded at 18.331 watt. From the FEMM calculation the core losses is registered at 19.31 watt as shown in Figure 6(a) and (b). The difference between experimental and FEMM computation is about 4.2%

Figure 6 (a) shows the flux legend through out the core that have maximum 2.09T induction in the center limb. The calculation had involved 39,431 nodes with 78,021 elements as depicted in Figure 6 (b) Previous work done by A. Basak [1] shows that the difference between experimental and computation is about 5.76% at 1.6T induction. The 4.2% difference is in good range and agreement with the previous work.

Form the flux movement in the core following the angular frequency incremental ωt of 30 degree, it is an obvious phenomenon that at any one time the flux is gradually emptying one of the limb while filling the other two limb. This can be seen from Figure 5 (d) to 5(g). It took about 180° electrical degree to migrate a pool of flux to the other two limb.

At any time there are two loops of flux flowing in the core which can be either two diferrent loops or two similar loops as shown in Table 3. At ωt = 30°, flux flow is maximum in the center limb.

ωt	0°	30°	60°	90°	120°	150°	180°
Flux flow	2 loops	2 loops	2 loops	2 loops	2 loops	2 loops	2 loops
Direction	Opposite	Opposite	Opposite	same	same	Same	same

Table 3

Similar work was done using FEM Quickfield 5.2 free version from the website but the problem cannot be solved due to limitation on the memory issues during mesh and nodal computation which limit to 250 mesh only.

Sinusoidal waveform is an important indicator to see the complete picture of flux movement under stable condition for CRGO material and possibly for other material as well.

From the flux flow legend, it is noted that the hot spot area in the core is in the inner corner of the core near the T joint and along side the core window as shown in Figure 6(a) at 1.7T induction level.

4. Conclusion

From this work, important findings that can be observed are :

a) FEMM 4.2 software is a user friendly software that can assist interested party to explore magnetostatic problems in transformers or other electrical machines.

It does not have any limitation on the formation of nodes like Quick Field 5.2 does. It will used maximum allowable memory available in the computer for the computation.

b) From the flux pattern, it took about 180° electrical degree for the flux to migrate to the other two limb in the transformer core.

c) There are two loops of flux flow at any ωt angle either in the form of oposite or same direction of flux flows.

d) The core loss differences between the experimental and computational is about 4.2% which is in good agreement with the previous work.

e) Hot spot area in the core is along the inner core corners near the T joint and along core windows

f) Sinusoidal waveform can be considered as a medium or tool to explore the behaviour of flux movement in CRGO material

References

[1] A. Basak, C.H.Yu, G. Llyod, " Core loss computation of a 1000 kVA distribution transformer" , Journal of Magnetisam and Magnetic Materials 133 (1994) 564-567

[2] Ed G. teNijenhuis, Jan Erik Wrethag, Kurt Gramm and Ramsis S. Girgis, " Experimental Investigation on Effect of Core Production Attributes on Transformer Core Loss Performance ", IEEE Transaction on Power Delivery, Vol. 13, No.2, April 1998, 526-531

[3] Daut I.,Dina M.M.Ahmad.,S.Zakaria, S.Uthman and S.Taib, "Comparison of Losses and Flux Distribution in 3 Phase 100 kVA Distribution Transformer Assembled From Various Type of T-joint Geometry", American Journal of Applied Science 3(9) ISSN 1546-9239 Science Publication 2006, 1990-1992

[4] FEMM version 4.2 User's Manual Feb.5.2009, pp 7-8

[5] Noraini Baser 'Undergraduate Project Paper' Uniten 2009

http://103.86.130.60/handle/123456789/21558

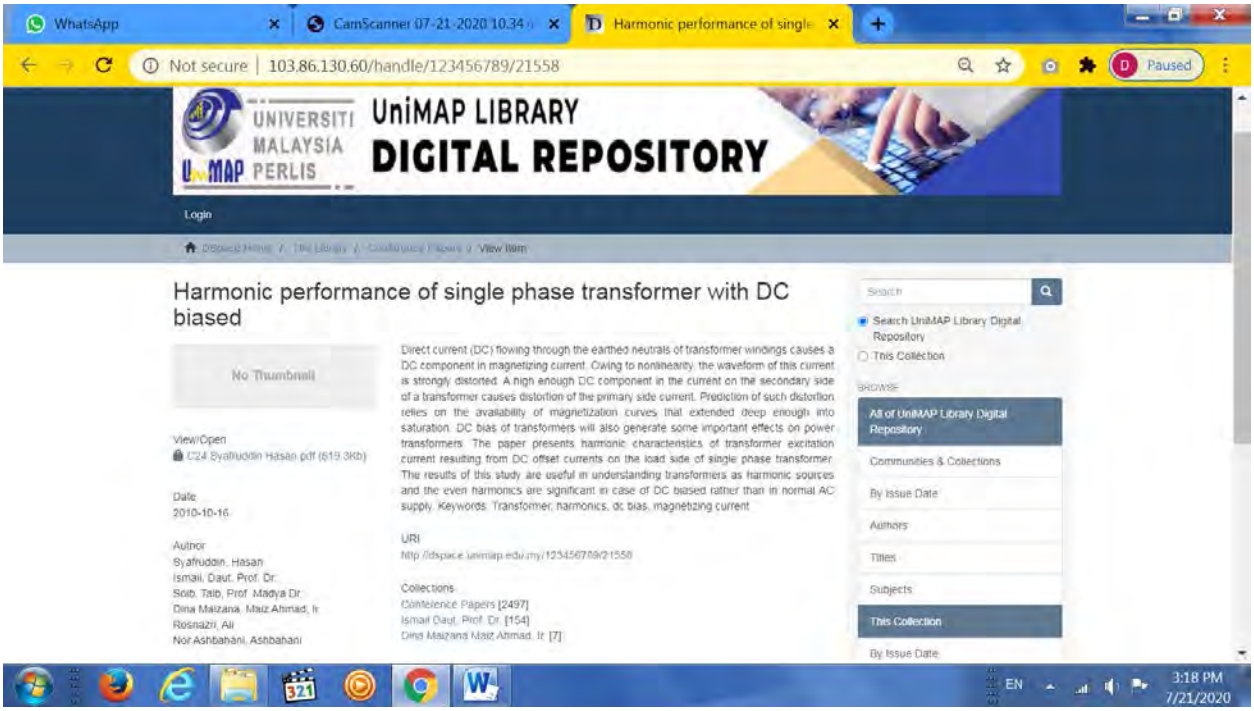

Proceedings of the International Postgraduate Conference on Engineering (IPCE 2010)
16 - 17 October 2010, Perlis, Malaysia

Harmonic Performance of Single Phase Transformer with DC Biased

Syafruddin Hasan, I.Daut, [1)]Soib Taib, Dina M., Rosnazri Ali, Nor Ashbahani
School of Electrical Systems Engineering
Universiti Malaysia Perlis (UniMAP)
E-mail:syafruddin@unimap.edu.my
[1)] *School of Electrical & Electronic Engineering*
Universiti Sains Malaysia (USM)
E-mail:soibtaib@eng.usm.my

Abstract

Direct current (DC) flowing through the earthed neutrals of transformer windings causes a DC component in magnetizing current. Owing to non-linearity, the waveform of this current is strongly distorted. A high enough DC component in the current on the secondary side of a transformer causes distortion of the primary side current. Prediction of such distortion relies on the availability of magnetization curves that extended deep enough into saturation. DC bias of transformers will also generate some important effects on power transformers. The paper presents harmonic characteristics of transformer excitation current resulting from DC offset currents on the load side of single phase transformer. The results of this study are useful in understanding transformers as harmonic sources and the even harmonics are significant in case of DC biased rather than in normal AC supply.

Keywords: *Transformer, harmonics, dc bias, magnetizing current*

1. Introduction

Geomagnetically Induced Current (GIC) flow on the earth surface due to Solar Magnetic Disturbances (SMD) which may also called Geomagnetic Disturbance (GMD), HVDC monopole transmission system, quasi-direct or direct current will flow into the nearby transformers whose neutral point is grounded. The DC current also could be due to power electronic operating under normal conditions or under abnormal conditions[1]. Depending on the level and duration of DC injection, possible adverse effects that may causes the saturation of transformer core during each half cycle. As a result, transformer magnetizing current will greatly increase and will be in rich in harmonics, which in turn could cause overall increase in transformer reactive power consumption [2]. Then some other problems can be generated, such as local overheating, the vibration and noise of the transformer, corrosion of grounding equipment, metering errors and malfunction of protective equipment which are directly related with the harmonic in the current of transformer [3][4].

This paper focuses on the prediction of magnetizing current distortion resulting from DC offset currents on the load side of single phase transformer. Therefore, the DC bias appears explicitly on the load side of the transformer model and formed part of the load current during laboratory testing

2. Transformer Operation with DC Bias

When a transformer is connected to a pure symmetrical load, the flux that is produced in the secondary will be opposed by the flux created from the additional component of primary current. Hence the mutual flux remains relatively unchanged. However, when the load current through that transformer is not perfectly symmetrical, which means the transformer is supplying a secondary current containing a DC component; a unipolar flux is established in the core.

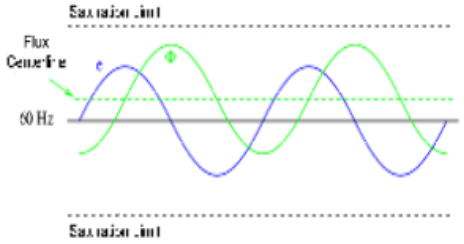

Figure 1 Flux waveform offset due to existence of DC bias

ISBN 978-967-5760-03-7

This unipolar flux is not opposed by the flux created from the additional component of primary current. It will add up with the mutual flux in the core and push the net flux in the core towards saturation. Consequently, the core is saturated during the half cycle in which the bias current is in the same direction as the magnetizing current [5]. This is depicted in Figure 1.

This additional flux "bias" or "offset" will push the alternating flux waveform closer to saturation in the positive cycle then the negative cycle. Therefore, the core material is said to experience half-cycle saturation [15]. The core material will enter half-cycle saturation earlier if the magnitude of DC component is greater; this is illustrated in Figure 2.

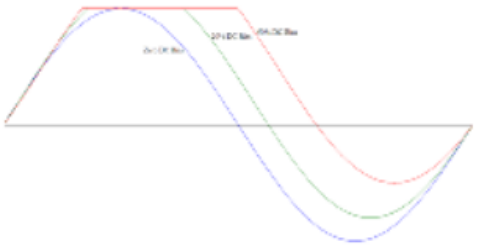

Figure 2 Flux waveform for various amounts of DC bias

3. Source of DC Bias

DC bias can originate from a number of sources, some of which are Geomatically Induced Currents (GIC), Photovoltaic Systems and AC and DC Drives.

3.1 Geomatically Induced Currents (GIC)

The interaction between solar wind and the Earth's magnetic field results in geomagnetic disturbances causing the flow of ionospheric currents known as electrojets. They occur at altitudes of 100 km or higher and have magnitudes of 1 x 10^6 A or more. They can change the Earth's magnetic field by as much as a few percent for several minutes. As a consequence, electric currents flow in the Earth, resulting in electric potential gradients. The ensuing potential differences between ground points drive geomagnetically induced currents (GICs) through power system facilities.

GICs are essentially direct currents that enter and leave the directly earthed neutrals of high-voltage star-connected windings, causing a DC bias in the magnetizing current of the transformer. The magnitudes of the transformer magnetizing currents are greatly increased and they will be rich in harmonics. The resulting DC bias in the core flux can be as high as 20% of the rated sine amplitude. Consequently, the core is saturated during the half cycle in which the bias current is in the same direction as the magnetizing current, triggering undesirable effects such as increased noise and additional core losses, as well [5].

GICs pose a threat to power system reliability. For example during the Great Geomagnetic Storm on 13 March 1989, the entire Hydro-Quebec system was plunged into a blackout, triggered by GIC, causing voltage collapse and equipment malfunction, infecting more than 6 millions consumers [6].

3.2 Photovoltaic Systems

Greenhouse gas concerns and desires for a more sustainable future are driving a rapidly expanding range of applications of grid connected distributed generation systems. These include photovoltaic systems. Many of these systems are interfaced to the grid via inverter systems which have characteristics and qualities unlike conventional synchronous or induction generators. PV systems that are connected via an inverter to the grid can cause a DC bias.

The two main issues with dc injection into the mains from equipment such as inverters are: (i) Differential mode injection i.e. between L-N or LL connections, and (ii) Common mode injection into both L and N connections causing earth leakage currents to flow.

The first mode of dc injection between line to line can lead to saturation of transformers supplying the particular circuit.

DC injection in an inverter without a 50Hz transformer can be caused by [7]:

- Unbalance in signals driving power devices connected direct to the mains. A small component is inevitable because there will always be some level of imbalance.
- Errors in measurement particularly zero errors which result in the control system outputting a small dc current to balance a zero error in the measuring transducer.
- Poor control resulting in hunting from half cycle to half cycle generating even order harmonics and dc components.
- Electronic circuit faults which result in loss of control. At least some transient dc current will be injected until a fault is detected and while the inverter shuts down.

3.3 AC and DC Drives

The application of variable-frequency drives (VFD) in industrial and commercial facilities has seen a tremendous increase in the last 2 decades. However, when multiple VFDs are fed from one dedicated power transformer, care should be taken not to drive the transformer into saturation.

Swamy & Rossiter had conducted an observation at an industrial location which has a cooling tower with nine ac induction motors rated at 150 hp each. The motors are retrofitted with VFD. The nine VFDs rated at 200 hp each are fed from a single 1500-kVA air-cooled transformer. According to their observation, the transformer showed saturation phenomenon, when it is feeding the VFDs. This has the potential of causing serious damage to the transformer. When all of the VFDs were run at the maximum output frequency of 60 Hz, the total input current and voltage harmonic distortion observed were high. The input ac current waveform was observed to be asymmetrical. The input ac current was uneven about the time axis. Large dc component close to 35% was observed in each phase. Even harmonic components as high as 47% were also present in the input current spectrum.

The severity of this DC injection will be dependent upon the type of conduction devices utilized (e.g. diodes and thyristors) and the quality of device matching. With respect to DC drives there a number of drive topologies that can inject significant components of DC. The half-wave rectifier is notorious for injection of DC however its practical use is limited. The three phase half controlled rectifier can also be a source of DC injection [8].

4. Model

The transformer test has the specification as single-phase power transformer with primary winding of 250 turns and secondary of 250 turns respectively. The dimension of the core is 508 mm x 306 mm with yoke and limb 100 mm width.

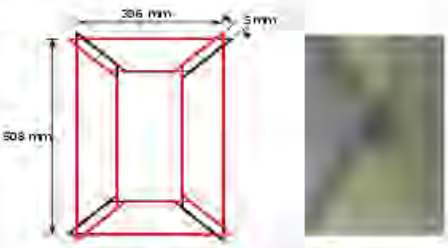

Figure 3 The arrangement of the core

The core is assembled from 0.27 millimeter thickness lamination of M4 grain-oriented silicon iron (CGO) that comprises of 15 layers and 5 mm corner overlap length configuration (shown in Figure 3)

The arrangement of equipment set-up which used in this research work is as shown in Figure 4. The input current to harmonic analyzer (PM 300) is connected to ac variable voltage variable frequency supply and its voltage is come from the secondary side of transformer test (transformer turn ratio 1:1). The experiment was conducted with different flux density by varying the input voltage and frequency.

Figure 4 Experimental Set up

The design philosophy of flux density variation that adopted here is derived directly from Faraday's and Ampere's laws. Equation (1) shows that the calculation of the primary voltage required to establish a predetermined flux density testing point, at a given frequency,

$$E_1 = 4.44\, N\, f\, B_{max}\, A \qquad (1)$$

where N is number of windings, f is supply frequency (Hertz), B_{max} is magnetic flux density in core (Tesla) and A is effective core area (m^2). Because of A is constant (can be calculated from core configuration),

$$A = n \times w \times t \qquad (2)$$

where n = number of core layer
w = core width (m)
t = core thickness (m)

and by assuming, that the input voltage equal to primary emf induced, the magnetic flux density can be varied by varying the input voltage, meanwhile the frequency is maintained constant.

5. Results

Laboratory experiment result of power factor of input current at various DC current injections for certain magnetic flux densities is shown in Figure 5.

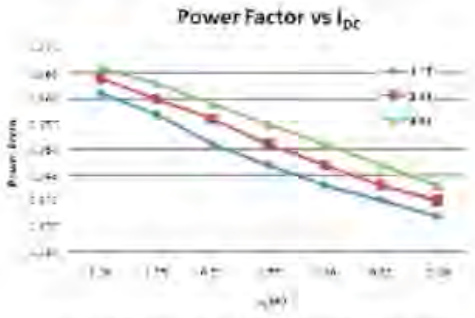

Figure 5 Power factors for various DC currents injection

The related secondary voltage crest factor for different DC currents injection is depicted as shown in Figure 6.

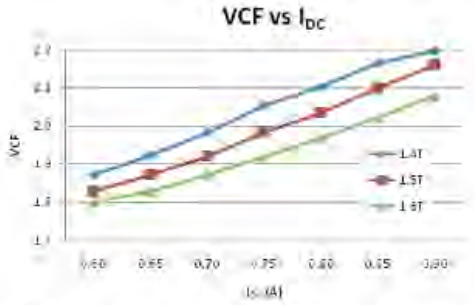

Figure 6 Secondary voltage crest factor for various DC currents injection.

In term of harmonic content, the current total harmonic distortion and individual harmonic distribution are displayed in Figure 7 and 8

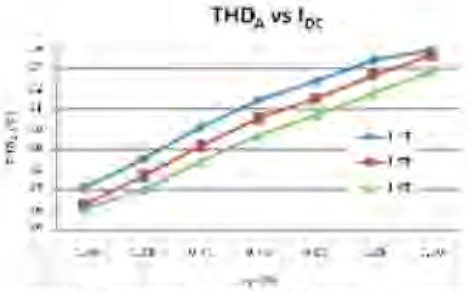

Figure 7 Current total harmonic distortion for various DC currents injection

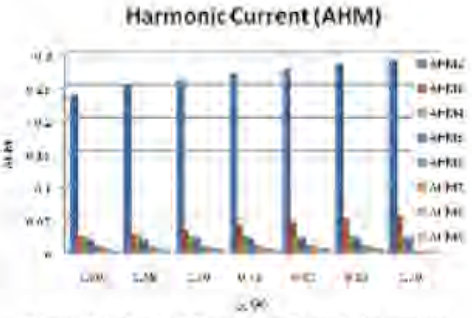

Figure 9 Individual Harmonic Current for various DC currents injection

6. Discussion

The knowledge of harmonics produced by DC biased transformers will be valuable resources in many applications. Several simplifications are made in this study. The winding loss and as well as the leakage inductances are not included in the excitation magnetic flux density calculation. All these approximations are considered to be of lower order affects.

Although we normally expect the voltage distortion to be very low compared to the current distortion, but with the exist of DC component, the power factors are decreased with DC current increase. These phenomenon are also related to the harmonics content as displayed in crest factor and THD_A.

By definition, a perfect sine wave current or voltage will have a crest factor of the square root of 2 or 1.414 and any deviation of this value represents a distorted waveform. Figure 6 shows the secondary voltage crest factors are higher than this condition. The crest factors are increase when the DC current injections increase.

It can be seen from current total harmonic distortion (THD_A) and individual harmonics distribution with respect to various DC current injections in Figure 8 and Figure 9 that the amplitude of the harmonics is increased with the DC bias current. At the same time, there are even harmonics and higher harmonics appeared.

7. Conclusion

The paper presents characteristics of transformer excitation current harmonics under DC bias on the load side of single phase transformer. Based on this study, the following observations can be made for this particular type of transformer.

- The harmonic contents are evaluated in term of crest factor (CF), total harmonic distortion (THD), individual harmonic distortion and power factor.
- Voltage crest factor, current total harmonic distortion and current individual harmonic are increase with DC bias increasing and vice versa with the power factor.
- Harmonics begin to appear at relatively low DC bias, and each harmonic will follow a certain pattern as the DC bias increases.

The second harmonic peaks only one as the DC bias level increases. The third harmonic shows two peaks with the increase of DC bias. The forth harmonic also shows a clear pattern.

References

[1] A.Ahfock and A.J.Hewitt, "DC Magnetization of Transformers", *IEE Proceeding Electric Power Applications*, 2005

[2] Y.You, E.F.Fuchs, and P.R.Barnes, "Reactive Power Demand of Transformer with DC Bias", *Industry Application Society Magazine*, Vol. 2, No. 4, July/August 1996, pp.45-52.

[3] Yinghui Chen, Tiebing Lu, and Zhibin Zhao, "Study on the Electromagnetic Influence of DC Bias on the Power Transformer", *IEEE Xplore…*

[4] Shu Lu, Yilu Liu, and Jaime De La Ree, "Harmonic Generated from a DC Biased Transformer", *IEEE Transaction on Power Delivery*, Vol.8, No.2, April 1993

[5] O.Biro, S.AuBerhofer, G.Buchgraber, K.Preis and W.Seitlinger, "Prediction of magnetising current waveform in a single-phase power transformer under DC bias", *IET Science Measurement Technology*, 2007, I. (1), pp. 2-5

[6] Grigsby L.L., "*The Electric Power Engineering Handbook*", CRS Press (2001)

[7] Spooner E.D., "*A New Australian Standard for Small Grid-Connected Renewable Generation System Connected via Inverters*", Australian CRC for Renewable Energy (ACRE), School of Electrical Engineering & Telecommunications, The University of New South Wales

[8] Swammy M. M., and Rossiter S.L., "Harmonic Interaction Between 1500 kVA Supply Transformer and VFD Load at an Industrial Plant", *IEEE transactions on Industry Application*, vol.34, No.5, 1998, pp. 897-903

http://103.86.130.60/handle/123456789/21237

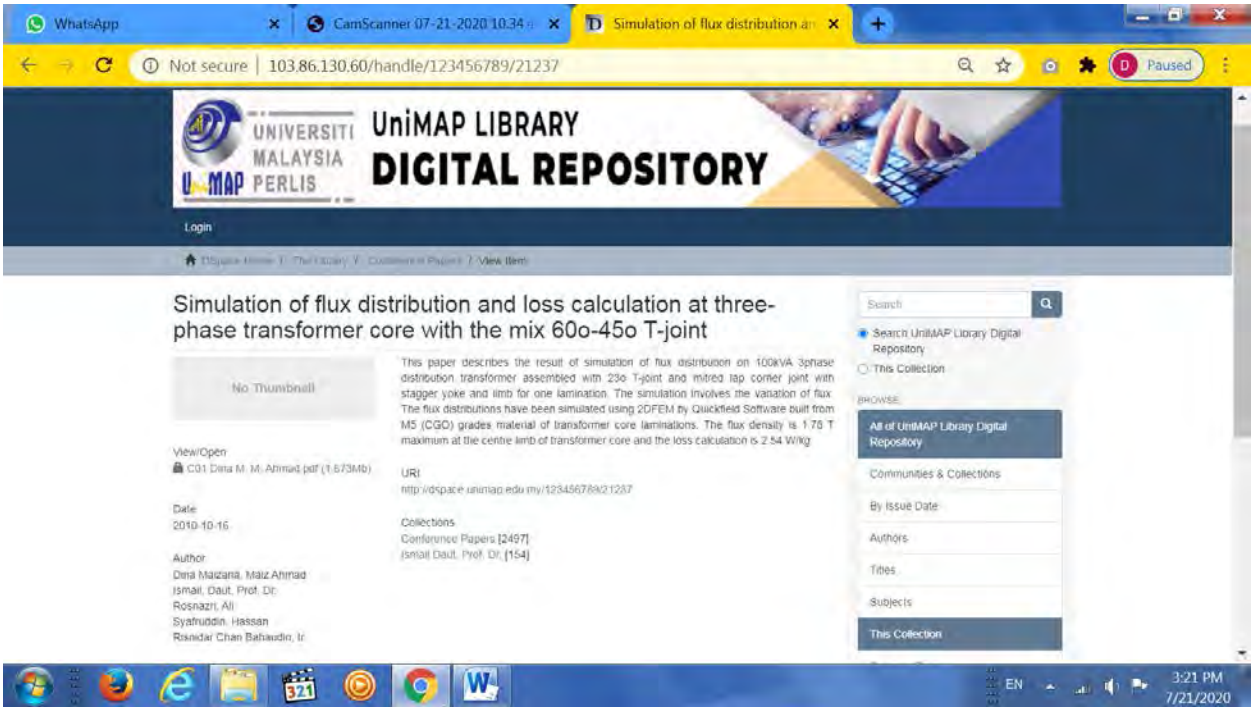

Proceedings of the International Postgraduate Conference on Engineering (IPCE 2010)
16 - 17 October 2010, Perlis, Malaysia

Simulation of Flux Distribution and Loss Calculation at Three-Phase Transformer Core with the Mix 60°-45° T-Joint

Dina M. M. Ahmad , I. Daut, Rosnazri Ali, Syafruddin Hassan and Risnidar C. B.
School of Electrical System Engineering, Universiti Malaysia Perlis (UniMAP),
P.O Box 77, d/a Pejabat Pos Besar
01007 Kangar Perlis, Malaysia
Email address: dina@unimap.edu.my, ismail.daut@unimap.edu.my

Abstract

This paper describes the result of simulation of flux distribution on 100kVA 3phase distribution transformer assembled with 23° T-joint and mitred lap corner joint with stagger yoke and limb for one lamination. The simulation involves the variation of flux. The flux distributions have been simulated using 2DFEM by Quickfield Software built from M5 (C'GO) grades material of transformer core laminations. The flux density is 1.78 T maximum at the centre limb of transformer core and the loss calculation is 2.54 W/kg.

Key words: Transformer core, flux distribution, power loss calculation, 2D FEM.

1. Introduction

The electrical transformer was invented by an American electrical engineer, William Stanley, in 1885 and was used in the first ac lighting installation at Great Barrington, Massachusetts. The first transformer was used to step up the power from 500 to 3000 V and transmitted for a distance of 1219 m (4000 ft). At the receiving end the voltage was stepped down to 500 V to street power and office lighting. By comparison, present transformers are designed to transmit hundreds of megawatts of power at voltages of 700 kV and beyond for distances of several hundred miles. [1]

Loss evaluation has become important because of high energy cost. Therefore, it is necessary to know in detail the behaviours of flux in transformer in order to develop cores with higher efficiency.

The efficient operation of power transformer cores depends to a large extent on the design of the joints between their limbs and yokes. In the three-phase, three limb core the most complex joints are the T-joints at the intersection the centre limb and yokes.[5]

The quantitative analysis of localized flux and loss distributions has become easier through the remarkable progress of numerical field calculations such as the finite element method. The numerical simulation is more effective and economical than experimental method. Moreover, useful suggestions for improving transformer can be obtained from the calculated flux and loss distribution.

The objective of this simulation is to know the flux distribution and calculate the losses occur on the transformer core with 23° T-joint built from M5 grade material using 2D FEM.

2. Methodology

Methodology that is used to complete this investigation had been divided into three major tasks:

1) Drawing transformer core assemble with 23° T-Joint and M5 grade material.
2) Simulation of the transformer core drawing.
3) Loss calculation for the transformer core material.

Drawing the transformer core configuration is the first step before doing the simulation. In this simulation, this drawing had been done using Quickfield v5.2 software. QuickField is an interactive environment for electromagnetic, thermal and stress analysis. In QuickField, it works with several types of documents: problems, geometry models, material libraries and others. QuickField can perform linear and nonlinear magnetostatic analysis for 2-D and asymmetric models. The program is based on a vector potential formulation.

Dimension of the 100kVA transformer core model are as figure 1. The configuration of T-Joint is drawing in Figure 2.

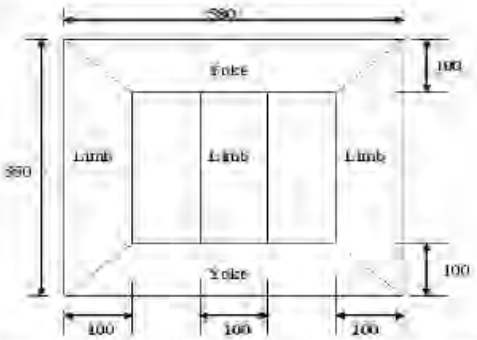

Φιγυρε 1. Διμενσιον (μμ) οφ 100κϖΑ τρανσφορμερ χορε μοδελ

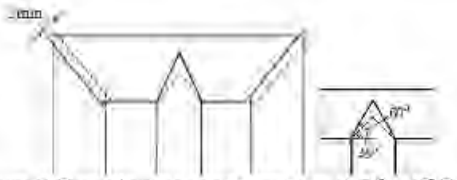

Φιγυρε 2. Τρανσφορμερ χορε τψπε τηε μιξ 60° – 45° T-φοιντ

ISBN 978-967-5760-03-7

To identify the material, B-H curve reading need to be tuck at the data column for each of the limb. The values for material can be obtained from the B-H curve. The data should be tucking as indicated in table 1.

Ταβλε 1: B–H χυρωε δατα φρομ της εξχιτινγ φορχε

Flux Density [T]	M5 grades, H (Am/g)
0.5	-130
0.6	-129.4
0.7	-129.2
1	-120
1.1	-116.5
1.3	-110.5
1.4	-96
1.5	-80
1.6	0
1.7	310
1.8	1870
1.8	9370

B-H curve data can be took from the hysteresis loop magnetizing curve of the material. Magnetizing curve for M5 grade material is obtained from the technical details of the CRGO material. Each of the limb and yokes block label need to be entering with the data such as coercive force of magnet, field source and others.

Directions of the coercive force of magnet are set to same to both of right and left limb. Only the centre limb are set different direction pole from the both right and left limb. In this drawing, the pole were set to be 90° for the right and left limb and the centre limb will be set to -90°. This will make sure flux from left and right limb will flow through the centre limb. Meanwhile for the upper yoke and lower yoke the direction were set to zero degree for both upper and lower yokes. [2]

After entering the related data for each of the block label properties, data label for edge also need to be set also. In this drawing, only air type and steel type need to be set for the edge label property. In the edge properties, for every edge of the steel need to be assign to tangential field and for the air edge, it need to be assign to magnetic potential

Before any simulation took place, the drawing should be check either mesh can produce all over the drawing or not as indicated in figure 3. There is button build mesh on top of the drawing toolbar. When building mesh is finish, the drawing will be cover with green line all over the drawing.

Simulation only can be executed after mesh had been built off. To execute the simulation, there is executing button on the toolbar icon. If the simulation success without having any error on the drawing a result with flux line flow through the core will come out. Value of flux density can be obtained from the field picture by right clicking on the result drawing. To check the local value, click on local value button and just pointing mouse at any space of the simulation result to get the result value.

Φιγυρε 3. Μεση βυιλδ.

3. Analysis

Flux Density formula

$$B = \mu H \quad (1)$$

$$\mu = \mu_r \mu_0 \quad (2)$$

where μ = material permeability
H = material intensity from the table

The flux density is assumed to lie in the plane of model (xy or zr), while the vector of electric current density **j** and the vector potential **A** are orthogonal to it. Only j_z and A_z in planar or j_φ and A_φ in axisymmetric case are not equal to zero. We will denote them simply j and A. Finally, the equation for planar case is

$$\frac{\partial}{\partial x}\left(\frac{1}{\mu_x}\frac{\partial A}{\partial y}\right)+\frac{\partial}{\partial y}\left(\frac{1}{\mu_y}\frac{\partial A}{\partial y}\right)=-j+\left(\frac{\partial H_y}{\partial x}-\frac{\partial H_x}{\partial y}\right) \quad (3)$$

and for axisymmetric case is

$$\frac{\partial}{\partial r}\left(\frac{1}{r\mu_r}\frac{\partial(rA)}{\partial y}\right)+\frac{\partial}{\partial z}\left(\frac{1}{\mu_r}\frac{\partial A}{\partial z}\right)=-j+\left(\frac{\partial H_r}{\partial z}-\frac{\partial H_z}{\partial r}\right) \quad (4)$$

where components of magnetic permeability tensor μ_x and μ_y (μ_r and μ_z), components of coercive force vector H_x and H_y (H_r and H_z), and current density j are constants within each block of the model.

In order to find the loss of energy per cycle or magnetization of transformer core lamination as follow;

Let l = mean of iron bar
A = its area of cross section
N = No of turns of wire of the solenoid.

with relate the B-H curve of core material shown in figure 4.

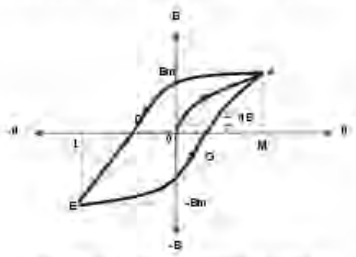

Φιγυρε 4. Ηψστερεσισ χυρωε

If B is the flux density at any instant, then $\Phi = BA$ when current through solenoid changes, then flux also changes and so produces and induced e.m.f whose value is

$$e = N\frac{d\Phi}{dt} volt \quad (5)$$

$$e = N\frac{d(BA)}{dt} = NA\frac{dB}{dt} volt \quad (6)$$

Now, $H = NI/l$ or $I = Hl/N$ (7)

The power of rate of expenditure of energy is maintaining the current '*I*' against induced e.m.f '*e*' is

$$= eI.watt = \frac{Hl}{N} \times N.A\frac{dB}{dt} = Al.H\frac{dB}{dt} \text{ Watt} \quad (8)$$

Energy spent in time '*dt*'

$$Al.H\frac{dB}{dt} \times dt = Al.H.dB \quad \text{Joule}$$

Total network done for one cycle of magnetization is

$$W = Al.\int H.dB \text{ Joule} \quad (9)$$

Hence $\int H.dB$ = area of the loop, i.e the area between B-H curve and the B-axis.

So, *work done, cycle* = *Al x (area of the loop)* Joule

Now *Al = volume of material*

So *net work done/cycle/m* = *(loop area)* Joule

Or *W = (area of B-H loop) joule/m³/cycle*

4. Result and Discussion

As an overview flux will flow through the core limb in various patterns. From figure 5 it shows that flux flow through centre limb from each left and right limb. Simulation using Quickfield software showing the flux lines flow through the limb and yoke of transformer core.

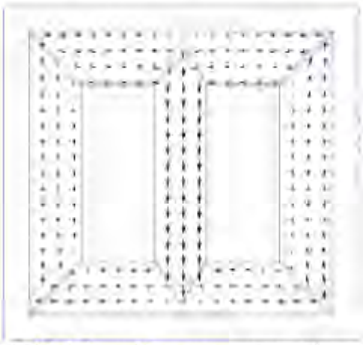

Φιγυρε 5. Φλυξ λινεσ φλοω τηρουγη τρανσφορμερ χορε

The flux density value from simulation is 1.78 T as indicated in figure 6. Flux density that is flow through the transformer core is not uniform. The maximum flux density is found in the centre limb of transformer core. Because the flux density that is flow from the left and right limb of the transformer core is enter toward the centre limb of transformer core.

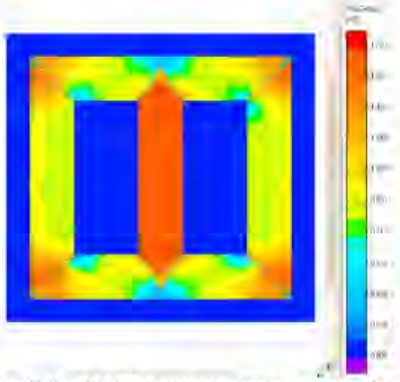

Φιγυρε 6. Τηε φλυξ δενσιτψ οχχυρ ιν τηε τρανσφορμερ χορε λαμινατιον

An energy density value is recorded in unit J/m³. For M5 grade material of the transformer core has the value of energy density is 384 J/m³. Energy density obtained from the simulation result is shown in figure 7. In this figure shows the energy density occurs at the left and right limb of transformer core.

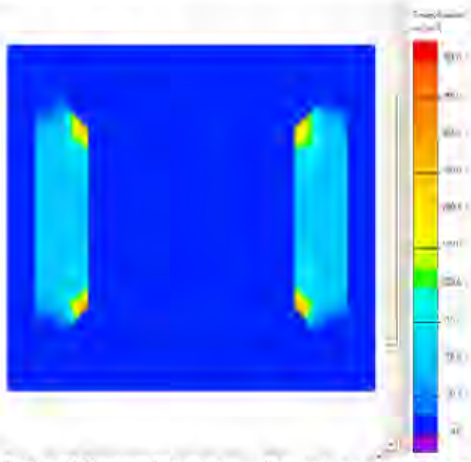

Φιγυρε 7. Ενεργψ δενσιτψ σιμυλατιονσ ον τρανσφορμερ χορε

From the simulation result, some data can be obtained such as;

Energy Density, ωH = 384 J/m³

Density = 7.65kg/dm³ (from the B-H curve)

In order to find frequency, the equation is,

$$f = \frac{1}{t} = \frac{1}{1\text{sec}} = 50Hz \Rightarrow t = \frac{1}{50}\text{sec} = 0.02\text{sec}$$

From simulation result data, power loss per kg can be calculated using;

$$Power.Loss/kg = \frac{384J/m^3}{7.65kg/dm^3} = \frac{384J/m^3}{7.65\times10^3 kg/m^3}$$

$$= \frac{384}{7.65\times10^3} J/kg \quad = \frac{384\times50}{7.65\times10^3} J/sec/kg \quad = 2.54Watt/kg$$

5. Conclusion

Loss evaluation has become important because of high energy cost. Therefore, it is necessary to know in detail the behaviours of flux in transformer in order to develop cores with higher efficiency.The values for material can be obtained from the B-H curve

From the result of simulation found the flux density is 1.78 T and the loss calculation is 2.54 W/kg. Flux density that is flow through the transformer core is not uniform. The maximum flux density is found in the centre limb of the transformer core.

6. References

[1]. Nakata, T., Numwrical Analysis of flux and loss distribution in Electrical Machinery (invited), *IEEE Trans. On Mag., Vol. MAG-20, no. 5* Sept. 1984.

[2]. Richard C. Dorf , *The Electrical Engineering Handbook*, 2nd Edition,CRC Press, pp: 32-35 1997.

[3]. I. Daut, Dina M.M. Ahmad, S. Zakaria, S. Uthman and S. Taib, Comparison of Losses and Flux Distribution in 3 phase 100kVA Distribution Transformer Assemble from Various Type of T-Joint Geometry, *American Journal of Applied Science* 3 (9):1990-1992, 2006

[4]. Gunther F. Mechler, Ramsis S.Girgis Magnetic Flux Distribution in Transformer Core Joints, *IEEE Transaction on Power Delivery Vol. 15,No 1*, Jan. 2000

[5]. Ismail Daut, Dina Maizana,Electrical Engineering Principle, Kolej Universiti Kejuruteraan Utara Malaysia (KUKUM) 2005.

[6]. Anthony J. Moses, Bleddyn Thomas, and John E. Thomson, Power Loss and Flux Density Distributions in the T-Joint of a Three Phase Transformer Core, *IEEE Trans. On Mag., Vol. MAG-8, no. 4* Dec 1972.

http://dspace.unimap.edu.my/handle/123456789/21229

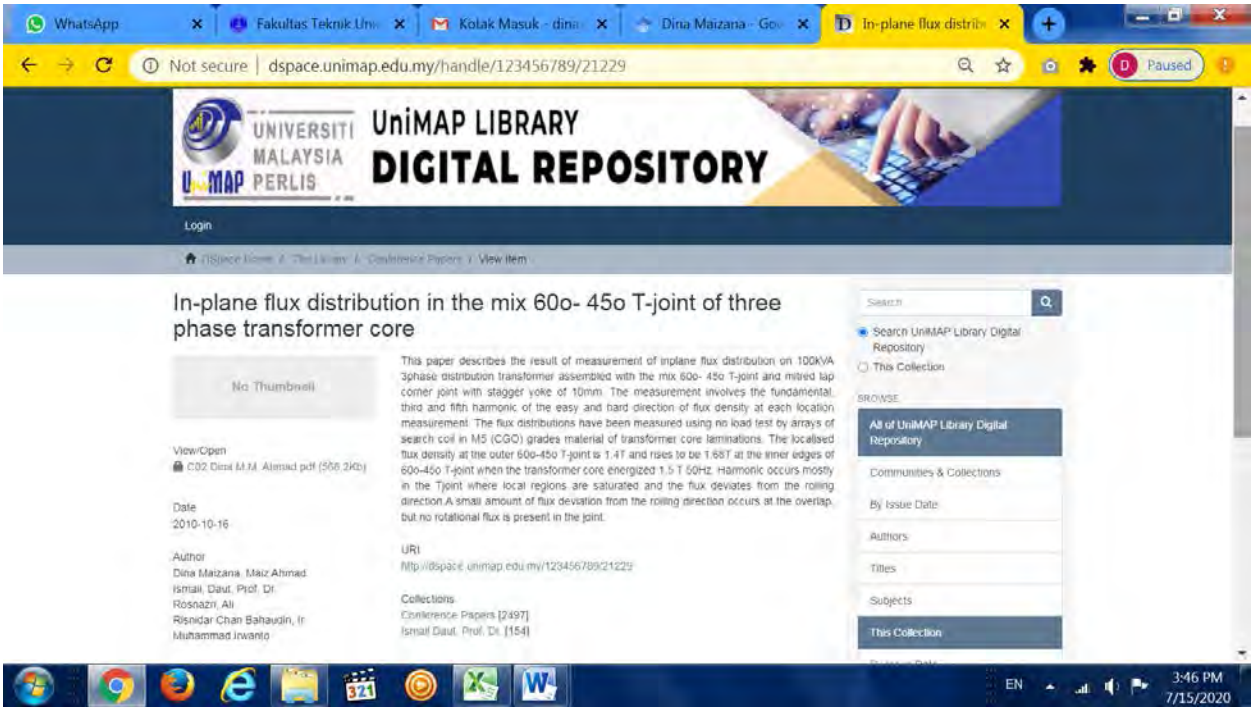

Proceedings of the International Postgraduate Conference on Engineering (IPCE 2010)
16 - 17 October 2010, Perlis, Malaysia

In-plane Flux Distribution in the Mix 60°- 45° T-joint of Three Phase Transformer Core

Dina M.M. Ahmad, Ismail Daut, Rosnazri Ali, Risnidar C.B. and M. Irwanto
School of Electrical System Engineering, Universiti Malaysia Perlis (UniMAP), Perlis, Malaysia,
dina@unimap.edu.my, ismail.daut@unimap.edu.my

Abstract

This paper describes the result of measurement of in-plane flux distribution on 100kVA 3phase distribution transformer assembled with the mix 60°-45° T-joint and mitred lap corner joint with stagger yoke of 10mm. The measurement involves the fundamental, third and fifth harmonic of the easy and hard direction of flux density at each location measurement. The flux distributions have been measured using no load test by arrays of search coil in M5 (CGO) grades material of transformer core laminations. The localised flux density at the outer 60°-45° T-joint is 1.4T and rises to be 1.68T at the inner edges of 60°-45° T-joint when the transformer core energized 1.5 T 50Hz. *Harmonic occurs mostly in the T-joint where local regions are saturated and the flux deviates from the rolling direction.A small amount of flux deviation from the rolling direction occurs at the overlap, but no rotational flux is present in the joint.*

Keywords—Distribution transformer, in-plane flux, third harmonic

1. Introduction

Transformer iron loss can be reduced either by improving the quality of the steel or by using better building and design techniques. The efficiency of a transformer core is also largely dependent upon the design of the joints at the junctions of the yoke and limbs. In these regions the flux may deviate from the rolling direction of the steel or become distorted so that local areas of the high loss are produced. [1] The use of grain-oriented silicon iron has been the main beneficial factor in increasing transformer efficiency. [2]

The behaviour of this investigation is to understand the in-plane flux distribution of the transformer core built from electrical steel (M5) with 3% silicon iron assembled with the mix 60°-45° T-joint and mitred lap corner joint with stagger yoke of 10mm by using arrays of search coil.

2. Experiment Apparatus and Measuring Techniques

The main apparatus consist of a model cores three-phase 100kVA transformer assembled with three limbs core with T-joint cutting angle the mix 60°-45° assembled from CRGO (M5 grades) 3% Si-Fe material. The core has 550 mm x 580 mm with the limbs and yokes 100 mm wide as shown in figure 1. The experimental cores assembled with the mix 60°-45° T-joint, mitred overlap corner joints with staggered yoke and overlap length is 10mm as shown in figure 2 and assembled from 0.3 mm thick laminations of M5 grain-oriented silicon iron (CRGO). Associated instruments are used to measurement fundamental, third and fifth harmonic content of the localised flux density distribution.

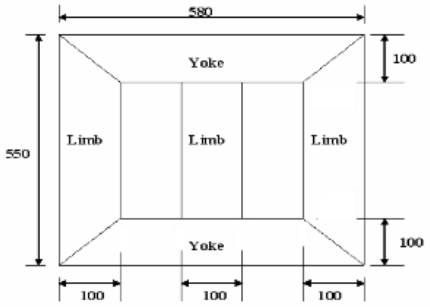

Φιγυρε 1. Δμενσιον (μμ) οφ 100κςΑ τρανσφορμερ μοδελ

The localized flux density distribution in individual laminations is measured using search coils. The samples are drilled with an aid of drilling machine. It is constructed from 0.15 mm diameter wire treaded through 0.8 mm diameter holes 10 mm a part as shown in Fig. 3. Each measuring position suitable coils are wound to measure the easy and hard direction flux density. The search coil induced voltages are analysed to find the magnitude and plane coil induced voltage of flux density by using power analyzer [PM6000] as shown in Fig. 4.

The magnitude and direction with reference to the x axis of the in-plane instantaneous flux density can be written in the form [3]:

$$|b| = \frac{1}{4fNAn}\left[e_x^{\,2} + e_y^{\,2}\right]^{1/2} \qquad (1)$$

And

$$\alpha = \tan^{-1}\left(\frac{e_y}{e_x}\right) \qquad (2)$$

ISBN 978-967-5760-03-7

Φιγυρε 1. Τρανσφορμερ χορε τψπε τηε μξ 60°– 45°Τ–φουρ τ

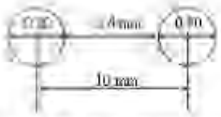

Φιγυρε 2. Δμενσιονσ [μμ] οφ τηε ηολεσ δριλλεδ ιν τηε σπ εχιμεν

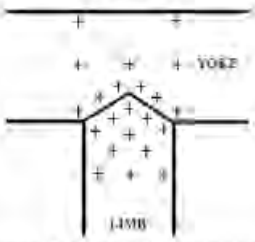

Φιγυρε 3. Λοχατιον οφ ορτηογοναλ σεαρχη χοιλσ ιν τηε τ ηρεε πηασε χορε

Where

f = frequency supply

N = Number of transformer winding

A = Cross section area of transformer core lamination that measured

n = number of layer of transformer core lamination

e_x = maximum value of the component of induced emf in the easy direction

e_y = maximum value of the component of induced emf in the hard direction

Sample calculation as follow:

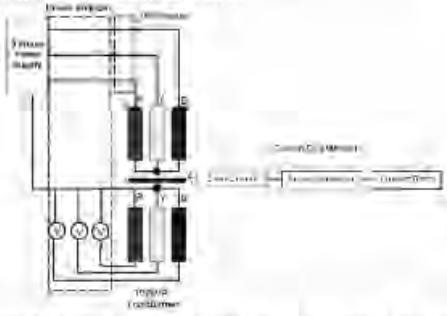

Φιγυρε 4. Τηε διαγραμοφ τηε μετηοδ τηατ υσεδ το μεασ υρε τηε λοχαλισεδ φλυξ δενσιτψ

From transformer frame are obtain number of turn is 254 turns, area of lamination is 0.000003m^2 with number of layer is 15 layers and frequency supply is 50 Hz. When the supply adjusted to transformer at 1.5T so at the search coil will find the induced emf by oscilloscope measurements at easy direction is 190mV and hard direction is 180mV. By using the equation (1) will find the flux density at this point is 103mT.

The primary induced emfs in the windings of the three phase transformers core were monitored by three identical voltmeters and voltages displayed during the measurement were only allowed to vary well within ± 0.4% of the induced voltage corresponding to the required flux density.

Flux distribution in the Cold Rolled Grain Oriented (CRGO) is measured by using an array of search coils to get the satisfactory result. In this investigation an array of single turn search coil is employed to measure in-plane (longitudinal and transverse) of flux density in the lamination within the transformer core as indicated in Fig. 3.Because the flux tends to deviate out of the longitudinal direction in some region, small 10mm search coils are used to measure localized longitudinal and transverse flux component. The locations are chosen to cover the areas where the flux is more likely to vary direction so as to find distribution of the flux behavior as shown in Fig. 5.

The testing process is done by using the No-Load Test Frame. The No-Load Test Frame consisting of three windings for each three phase core are designed in order not only to avoid introducing stress to the laminations but also to keep the magnetism exactly constant in all limbs of the cores. Each winding only extends along 85% on each limb in order to enable the stagger length of the three phase core to be varied. An extra softwood base 200mm high is used to raise the overall height of the core, in order to minimize the effect of the stray flux on the localized measurements.

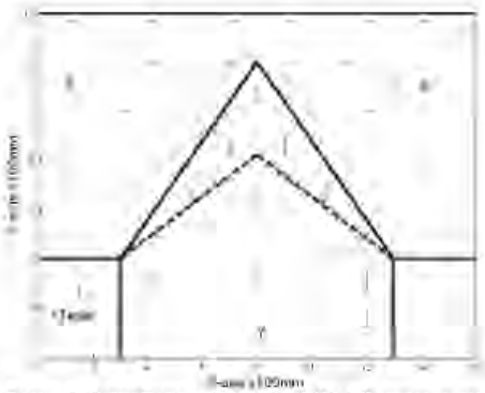

Φιγυρε 4. Διστριβυτιον οφ λοχαλιζεδ φλυξ δενσιτψ ον τηε μξ 60°–45° ιν δυφφερεντ λαψερσ οφ Τ–φουντ οφ τηρεε πηα σε χορε ατ δυφφερεντ ινστανταν ιν τιμε ωηεν θ=60°

Installation search coil takes quite a long time in completing this step which every hole needs to be inserted with search coil. Search coil is the enamel copper coated 0.1mm diameter wire. Each set of test point (4 holes) consist of easy and hard direction where the holes of easy and hard direction will be inserted search coil and the leads are twisted together. All the holes at testing point

need to be repeated the same method of inserting and twisting the leads.

After the search coils are wound and the leads twisted together, the holes are filled with polyurethane varnish to give added insulation protection. The search coil leads, which are twisted to prevent any spurious pick up, are stuck to the lamination by a polyurethane varnish. The leads from all the search coils are taken to a junction box placed in the core to prevent any interference from the core or magnetising windings.

3. Results and Discussion

The instantaneous magnitude and direction of flux at this instant is shown in Fig. 6 on a larger scale. At this instant the total flux in the centre limb reaches its maximum and outer limb carry half their maximum flux. A small amount of flux deviation from the rolling direction occurs at the overlap.

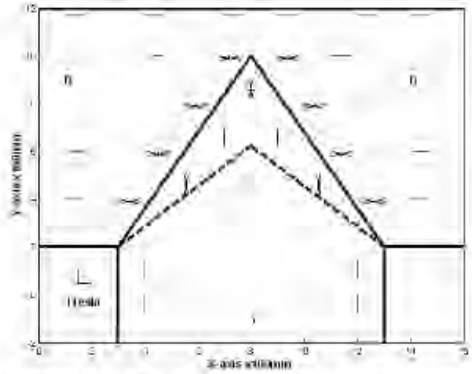

Φιγυρε 7. Λοχυσ οφ τηε φυνδαμενταλ χομπονεντ οφ λοχαλισεδ φλυξ δενσιτψ ιν τηε μιξ 60°–45° Τ-φοιντ σταγγερεδ χορεσ ωιτη οπερλαπ λενγτη 10 μματ 1.5Τ, 50Ηζ

The rotational flux produced in the T-joint region of the three-phase three limbs transformer core are due to a combined effect of alternating and rotating fields. This rotational flux illustrates the locus of the variation of the variation of the localized flux distribution throughout the magnetizing cycle. The rotational flux of the fundamental component (50Hz) of flux density in the 10mm staggered core at a core flux density of 1.5T is shown in Fig. 7. A large rotational flux is present in the yoke area which near with centre limb. Rotational flux in this region is more circular. Some large rotational flux is also observed in or near the T-joint region.

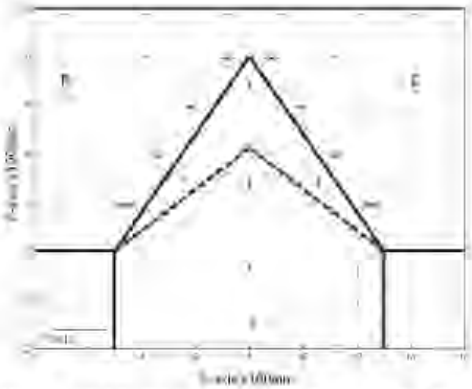

Φιγυρε 8. Λοχυσ οφ τηε τηιρδ ηαρμονιχ χομπονεντ οφ λοχαλισεδ φλυξ δενσιτψ ιν τηε μιξ 60°–45° Τ-φοιντ σταγγερεδ χορε ωιτη οπερλαπ λενγτη 10 μματ 1.5Τ, 50Ηζ

Fig. 8 shows the rotational flux of the third harmonic component of flux density in the T-joint of the core assembled with the mix 60°-45° T-joint at core flux density of 1.5T. The extent of rotating flux at this frequency is more widespread. As with the 50Hz component, a large amount of rotating flux is present in the T-joint region between the right yoke and centre limb in all four cores. A small rotating flux occurs also observed in the middle of centre limb region in all four cores. There is more rotational flux present in this region.

The major axes of the locus do not always follow those of the fundamental component (particularly the the mix 60°-45° T-joint of core) but tend to be parallel to butt joints over much of the core where the fundamental components also deviate from the longitudinal direction of the strip in the yoke.

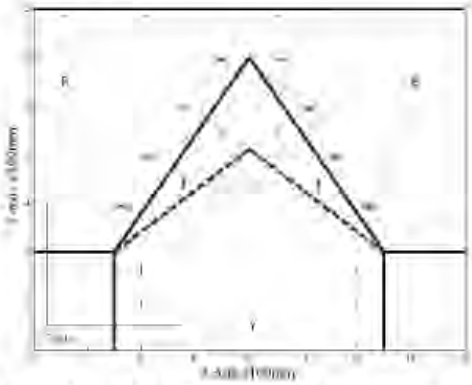

Φιγυρε 9. Λοχυσ οφ τηε φιφτη ηαρμονιχ χομπονεντ οφ λοχαλισεδ φλυξ δενσιτψ ιν τηε μιξ 60°–45° Τ-φοιντ σταγγερεδ χορε ωιτη οπερλαπ λενγτη 10 μματ 1.5Τ, 50Ηζ

Fig. 9 shows that the rotational flux of the fifth harmonic component of flux density in the T-joint of the

core assembled with the mix 60°-45° T-joint at core flux density of 1.5T is more widespread. The magnitude of the rotational flux is small compared with that of the fundamental and third harmonic. The distribution of the fifth harmonic component is classified to a region near to and within the T-joint.

A large amount of rotating flux is present in the T-joint region between the right yoke and centre limb in the core. Rotating flux in this region is elliptical with the the mix 60°-45° T-joint of core showing the highest value. A small rotating flux occurs also observed in the middle of centre limb region in the core.

Fig. 10 shows the measuring point of location and localized flux densities at the mix 60°-45° T-joint that are measured by using the search coil on transformer core. This result is produced by calculating localized flux density after the search coil measures the vector of the voltage in the easy and hard direction at the lamination.

The flux density in the yoke then drops rapidly as the flux distributes itself equally between the laminations. The flux density reaches a peak at the inner of the mix 60°-45° T-joint; this is caused by the saturated material. The minimum flux density occurs at the outer of the mix 60°-45° T-joint of transformer core lamination. The localised flux density will increase from the outer to the inner edge of the the mix 60°-45° T-joint. The localised flux density at the outer the mix 60°-45° T-joint is 1.4T and rises to be 1.68T at the inner edges of yoke at the mix 60°-45° T-joint when the transformer core energized 1.5 T 50Hz.

The local variation in magnitude of the third harmonic component of peak in-plane flux density in the mix 60°-45° T-joint at a core flux density of 1.5T is shown in Figure 11. Most of the high third harmonic flux occurs in the T-joint region. The high third harmonic of peak in-plane flux occurs at the inner edge of right yoke passes over to the Butt-joint of centre limb is 0.23T. Harmonic occurs mostly in the T-joint where local regions are saturated and the flux deviates from the rolling direction. However, it has been confirmed experimentally that harmonics circulated in individual laminations in the limbs and yokes.

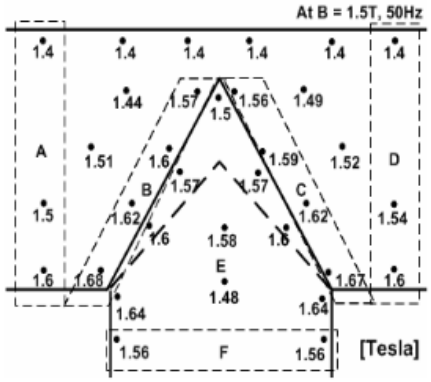

Φιγυρε 10. Λοχαλ ωαριατιονσ ιν τηε Τοφ τηε φυνδαμενταλ πεακ φλυξ δενσιτψ το τηε φυνδαμενταλ χομπονεντ ιν−πλανε οφ τηε λαμιναττιον ιν τηε μξ 60°−45° Τ−φοιντ οφ τηρεε πιεσε σταγγερεδ χορε ωιτη οωερλαπ λενγτη 10 μματ 1.5Τ, 50Ηζ.

The local variation in magnitude of the fifth harmonic component of peak in-plane flux density in the the mix 60°-45° T-joint at a core flux density of 1.5T is shown in Fig. 12 to be very small.

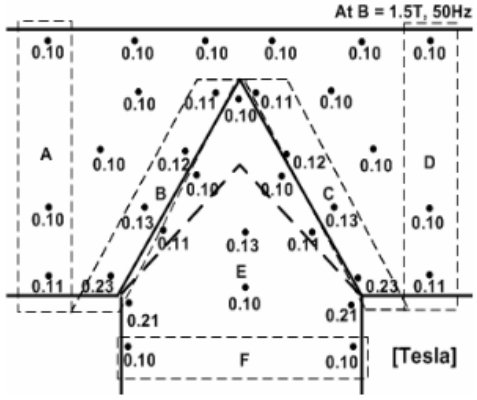

Φιγυρε 11. Λοχαλ ωαριατιονσ ιν Τοφ τηε τηιρδ ηαρμονιχ πεακ φλυξ δενσιτψ το τηε φυνδαμενταλ χομπονεντ ιν−πλανε οφ τηε λαμιναττιον ιν δυφφερεντ Τ−φοιντ οφ τηρεε πιεσε σταγγερεδ χορε ωιτη οωερλαπ λενγτη 10 μματ 1.5Τ, 50Ηζ.

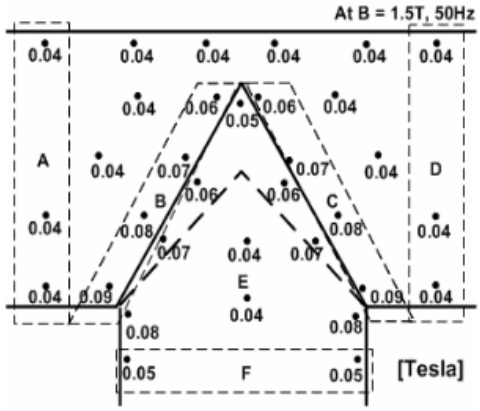

Φιγυρε 12. Λοχαλ ωαριατιονσ ιν Τοφ τηε φιφτη ηαρμονιχ πεακ φλυξ δενσιτψ το τηε φυνδαμενταλ χομπονεντ ιν−πλανε οφ τηε λαμιναττιον ιν δυφφερεντ Τ−φοιντ οφ τηρεε πιεσε σταγγερεδ χορε ωιτη οωερλαπ λενγτη 10 μματ 1.5Τ, 50Ηζ.

4. Conclusion

The flux distribution in cores assembled with M5 material was found varies along overlap area of the stagger at the T-joint. The localised in-plane flux density will increase from the outer to the inner of the the mix

60°-45° T-joint. The localised flux density at the outer edges the mix 60°-45° T-joint is 1.4T and rises to be 1.68T at the inner edges of the mix 60°-45° T-joint when the transformer core energized 1.5 T 50Hz. A large rotational flux is present in the yoke area which near with centre limb. Rotational flux in this region is more circular.

The high third harmonic of peak in-plane flux occurs at the inner edge of right yoke passes over to the Butt-joint of centre limb is 0.23T.Harmonic occurs mostly in the T-joint where local regions are saturated and the flux deviates from the rolling direction.

A small amount of flux deviation from the rolling direction occurs at the overlap, but no rotational flux is present in the joint.

The local variation in magnitude of the fifth harmonic component of peak in-plane flux density in the the mix 60°-45° T-joint at a core flux density of 1.5T is to be very small

5. References

[1] Jones, A. J., Moses, A. J., Comparison of the Localized Power Loss and Flux Distribution in the Butt and Lap and Mitred Overlap Corner Configurations, *IEEE Trns. ON MAG., VOL. MAG-10*, No. 2, june 1974.

[2] Mansel A Jones and Antony J. Moses, Comparison of the Localized Power Loss and Flux Distribution in the Butt and Lap and Mitre Overlap Corner Configurations, *IEEE Trans. On Mag., Vol. MAG-10*, No 2, June 1974

[3] Daut, I and Moses, A.J., Some Effects Of Core Building On Localised Losses And Flux Distribution In A Three-Phase Transformer Core Assembled From Powercore Strip, *IEEE Trans. On Mag., Vol. MAG-26*, No 5, pp. 2002, Sept 1990

[4] Daut, I.,"*Investigation of Flux and Loss Distribution in Transformer Cores Assembled From Amorphous Powercore Material*", 1992, PhD Thesis University of Wales

[5] Beckley P., *Electrical Steels for rotating machines*, The Institution of Electrical Engineers, 2002.

[6] Indrajit Dasgupta, *Design of Transformers Handbook*, Tata Mc-Graw Hill, India, 2002.

[7] James H. Harlow, *Electric Power Transformer Engineering*. CRC Press LLC, 2004.

[8] Daut I., Dina M.M. Ahmad and S. Taib, Measurement of flux distribution on 100kVA 3phase distribution transformer assembled with 60° T-joint and mitred lap corner joint with stagger yoke by using search coil, MUCET2008 8th-10th March 2008, Hotel Putra Palace, Perlis, Malaysia.

[9] Daut, Dina M.M. Ahmad, and S. Taib , Measurement of Flux Distribution on 100kVA 3phase Distribution Transformer Assembled With 45° T-Joint And Mitred Lap Corner Joint With Stagger Yoke By Using Search Coil, IASTED AsiaPES2008, 2nd-4th April 2008, Meritus Pelangi Beach Resort Hotel, Langkawi, Malaysia, ISBN CD: 978-088986-732-1

[10] Daut, Dina M.M. Ahmad, and S. Taib , Comparison Between The Localized Power Loss and Flux Distribution in a Three Phase Distribution Transformer 100 kVA Assembled From Various Type of T-Joint Geometry with Staggered Yoke, IASTED AsiaPES2008, 2nd-4th April 2008, Meritus Pelangi Beach Resort Hotel, Langkawi, Malaysia, ISBN CD: 978-088986-732-1,

[11] Dina M.M. Ahmad, Ismail Daut, Measurement of Flux Distribution on 100kVA 3phase Distribution Transformer Assembled With 23° T-Joint and Mitred Lap Corner Joint with Stagger Yoke by Using Search Coil, The 2ndInternational Power Engineering and Optimization Conference (PEDCO2008), Shah Alam, Selangor, MALAYSIA. 4-5 June 2008.

http://103.86.130.60/handle/123456789/21207

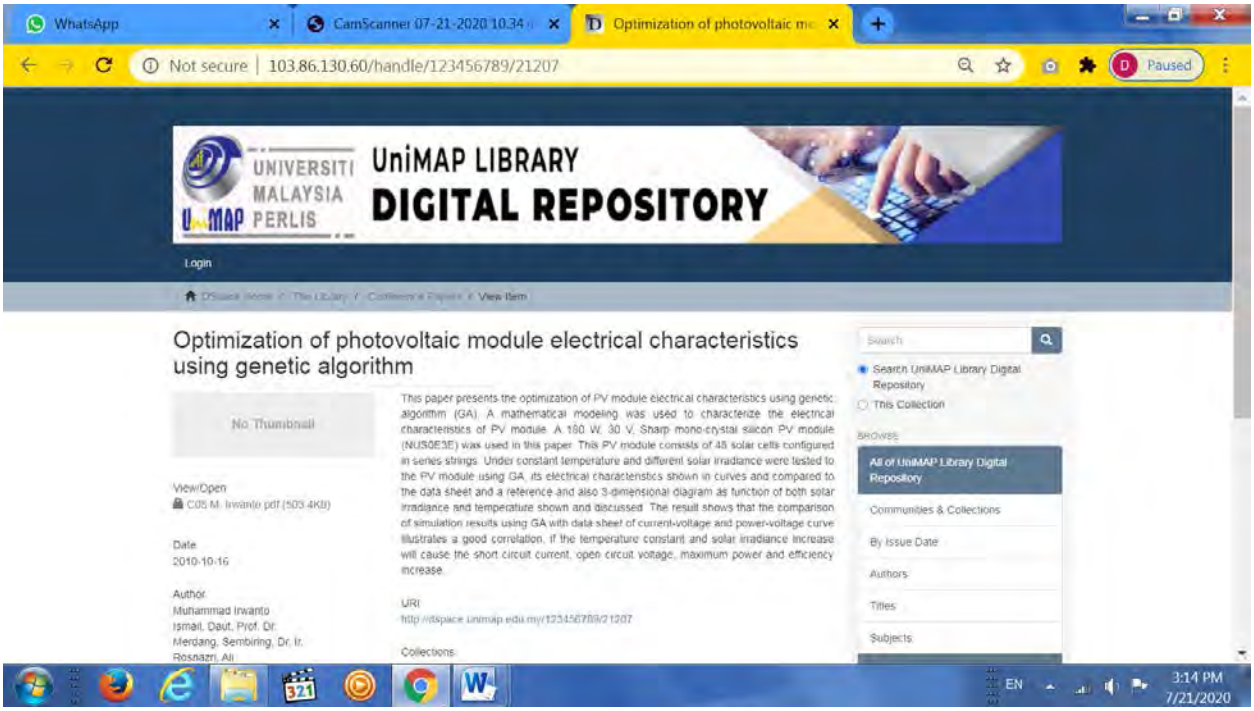

Proceedings of the International Postgraduate Conference on Engineering (IPCE 2010)
16 - 17 October 2010, Perlis, Malaysia

Optimization of Photovoltaic Module Electrical Characteristics Using Genetic Algorithm

M. Irwanto* , I Daut* , M. Sembiring** , Rosnazri Bin Ali *, Surya Hardi *, and Dina Maizana*
* *Cluster Power Electronic and Machine Design, School of Electrical System Engineering, University Malaysia Perlis (UniMAP), Malaysia*
Email: irwanto@unimap.edu.my
** *School of Mechatronic Engineering, University Malaysia Perlis (UniMAP), Malaysia*
Email: merdang@unimap.edu.my

Abstract

This paper presents the optimization of PV module electrical characteristics using genetic algorithm (GA). A mathematical modeling was used to characterize the electrical characteristics of PV module. A 180 W, 30 V, Sharp mono-crystal silicon PV module (NUS0E3E) was used in this paper. This PV module consists of 48 solar cells configured in series strings. Under constant temperature and different solar irradiance were tested to the PV module using GA, its electrical characteristics shown in curves and compared to the data sheet and a reference and also 3-dimensional diagram as function of both solar irradiance and temperature shown and discussed. The result shows that the comparison of simulation results using GA with data sheet of current-voltage and power-voltage curve illustrates a good correlation, if the temperature constant and solar irradiance increase will cause the short circuit current, open circuit voltage, maximum power and efficiency increase.

Keywords—Solar irradiance; Temperature; PV module; electrical characteristics; Genetic algorithm

1. Introduction

The major factors which influence the electrical design of the PV module are solar irradiance, tilt angle of PV module, load matching for maximum power and operating temperature [1]. The electrical characteristics of the PV module are generally represented by the current versus voltage (i-v) curve. The electrical characteristics of a PV module are influenced by temperature and solar irradiance, and they influence on the design of PV module system [2].

Temperature is an important consideration in the operation of PV module system [3]. At lower temperatures, PV module systems produce more power. For higher temperature, optimum operation requires modification of electrical load and removal of excess heat. At high temperatures, two predominating effects can cause efficiency to drop. As thermal energy increases, lattice vibrations interface with the free passing of charge carries and the junction begins to loss its power to separate charges.

The efficiency losses for PV systems can be minimized in the presence of temperature variations. In most cases, good solutions are a temperature-dependent charge controller or a maximum power tracker. Both devices improve the overall system efficiency at higher temperature where the performance is poor [3].

A c-Si module has been test to get its electrical characteristic by [4], 1000 W/m^2 of solar irradiance and temperature from 15 ^{0}C to 65 ^{0}C were fallen to the surface of the PV module. Its electrical characteristic was observed, the result shown that for solar irradiance was constant and temperature increased, its short circuit current would be constant, open circuit voltage and maximum power would decrease. Effect of temperature on electrical characteristic of a photovoltaic module has been tested by [2], shown that for 975.4 W/m^2 and temperature were 25.1 ^{0}C, 45.9 ^{0}C and 55.6 ^{0}C resulted the maximum power were 44.98 W, 40.06 W and 38.11 W, respectively. The open circuit voltage varies linearly with temperature if the temperature were increased [5].

Constant temperature of 25 ^{0}C, and solar irradiance of 600 W/m^2, 800 W/m^2, 1000 W/m^2 (increased

ISBN 978-967-5760-03-7

solar irradiance) were tested to a c-Si PV module by [4], the result shown that the short circuit current, open circuit voltage, and maximum power would increase. The effect of solar irradiance on a photovoltaic module performance was tested by [2] also, shown that for 37.7 ^{0}C of constant temperature, solar irradiance were 626 W/m^2, 831 W/m^2 and 974 W/m^2 resulted the maximum power were 28.27 W, 36.55 W and 41.85 W, respectively. Research by [5] shown that the short circuit current increases almost linier, the fill factor is not significantly influenced by the solar irradiance, the maximum power point varies sub linearly with solar irradiance.

A behavioral model has been developed by [6] to characterize current, voltage and power of photovoltaic modules as function of solar cell temperature and solar irradiance. Calculated diagrams are compared with diagrams of two photovoltaic module data sheet.

Genetic algorithms have proved to be a versatile and effective approach for solving optimization problem [7]. A genetic algorithm is used to design the hybrid system optimally [8], the hybrid system is composed of photovoltaic cells, a battery, and a fuel cell supplying a stand-alone street lighting system.
This paper presents a mathematical modeling to observe PV module electrical characteristics. A mono-crystal silicon PV module was tested under constant temperature and different solar irradiance using GA,. The observed PV module performances are the short circuit current, the open circuit voltage, the maximum power, the fill factor and the efficiency.

2. Methodology

2.1. Mathematical Modeling of PV Module Electrical Characteristics

The most popular photovoltaic module is a particular case of a series string of solar cells. In terrestrial application the PV standard modules are composed of a number solar cells connected series. The number is usually 33 to 36 but different association also available [10]. The mathematical modeling of circuit current and open circuit voltage of a PV module electrical characteristic follow what was proposed by [6], using GA the circuit current timed by range of the open circuit voltage to produce power and maximum power of the PV module.

To use this model it is required to know open module voltage $V_{\min}$ and $V_{\max}$ in two operation points with different solar irradiance levels $\alpha_{\min}$ (e.g. 200 W/m^2) and $\alpha_{\max}$ (1000 W/m^2) at the same nominal temperature T_N (25 ^{0}C). In addition to these four parameters, the model requires additional five parameters from a PV module data sheet that are the short circuit current I_{sc}, voltage V_{MPP} and current I_{MPP} in the maximum power point all at STC as well as the temperature coefficients of the short circuit current TC_i and open voltage TC_v. The parameters "b" is the fit parameter of the PV model. It influences the I-V curve in the maximum power point. The circuit current $I(\alpha,T,V)$ and open circuit voltage $V_{oc}(\alpha,T)$ as function of solar irradiance, temperature and voltage are given by [6]

$$I(\alpha,T,V) = \frac{\alpha}{1000\frac{W}{m^2}}.I_{sc}.\tau_i(T).\left[\frac{1-e^{\left[\frac{V}{b\left(1+\frac{V_{\max}-V_{\min}}{V_{\max}}.\frac{\alpha-\alpha_{\max}}{\alpha_{\max}-\alpha_{\min}}\right).(V_{\max}+\tau_v(T))}\right]^{-\frac{1}{b}}}}{1-e^{-\frac{1}{b}}}\right] \quad (1)$$

When $I(\alpha,T,V) = 0$ A, the open circuit voltage is given by

$$V_{oc}(\alpha,T) = \left[1+\frac{V_{\max}-V_{\min}}{V_{\max}}.\frac{\alpha-\alpha_{\max}}{\alpha_{\max}-\alpha_{\min}}\right].\left[V_{\max}+\tau_v(T)\right] \quad (2)$$

$$\tau_i(T) = 1+\frac{TC_i}{100\%}.(T-T_N) \quad (3)$$

$$\tau_v(T) = TC_v.(T-T_N) \quad (4)$$

2.3. Solar Irradiance Effect

The open circuit voltage can be given by [7]:

$$V_{oc} = V_T \ln\left(1+\frac{I_{sc}}{I_0}\right) \quad (5)$$

From (5), it can be seen than the value of the open circuit voltage depends, logarithmically on the I_{sc}/I_o ratio. This means that under constant temperature the value of the open circuit voltage scales logarithmically with the short circuit which, in turn scales linearly with irradiance resulting in a logarithmic dependence of the open circuit voltage with irradiance. This is also an important result indicating that the effect of the irradiance is much larger in the short circuit current than in the open circuit value.

2.4. Photovoltaic Module Characteristics

In this paper the photovoltaic module characteristics are [11]:

1. Short Circuit Current (I_{SC})

The short circuit current (I_{SC}) represent to the maximum current ($I_{\max}$) that passes through the cell that corresponds to the short circuit condition when the impedance is low. It occurs at the beginning of the sweep when the voltage is zero. In an ideal cell, this maximum current value is the total current produced in the solar cell by photon excitation.

$$I_{SC} = I_{\max} \text{ , at } V = 0 \tag{6}$$

2. Open circuit voltage (V_{OC})

The open circuit voltage (V_{OC}) is the maximum voltage difference across the cell, and it occurs when there is no current passing through the cell.

$$V_{OC} = V_{\max} \text{ , at } I = 0 \tag{7}$$

3. Maximum power ($P_{\max}$)

The power produced by the cell in watts can be easily calculated along the I-V characteristic curve. At the I_{SC} and V_{OC} points, the power will be zero and the maximum value for power will occur between the two points. The voltage and current at this maximum power point are denoted as $V_{\max}$ and $I_{\max}$ respectively.

$$P_{\max} = V_{\max} x I_{\max} \tag{8}$$

4. Fill factor (FF)

The Fill Factor (FF) is essentially a measurement of quality of the solar cell. It is calculated by comparing the maximum power to the theoretical power (P_T) that would be output at both the open circuit voltage and short circuit current together. FF can also be interpreted graphically as the ratio of the rectangular areas, its larger desirable, and corresponds to an I-V characteristic curve. Typical fill factors range from 0.5 to 0.82.

$$FF = \frac{P_{\max}}{P_T} = \frac{V_{\max} x I_{\max}}{V_{OC} x I_{SC}} \tag{9}$$

5. Efficiency (η)

Efficiency is the ratio of the electrical power output (P_{out}), compared to the solar power input (P_{in}) into the PV cell. P_{out} can be taken to be $P_{\max}$ since the solar cell can be operated up to its maximum power output to get the maximum efficiency.

$$\eta_{\max} = \frac{P_{\max}}{P_{in}} \tag{10}$$

2.5. PV Data

A 180 W, 30 V, Sharp mono-crystal silicon PV module (NUS0E3E) was used in this paper [9]. This PV module consists of 48 solar cells configured in series strings. The complete data sheet of the PV module is shown in Table 1.

Table 1. Electrical parameters of mono-crystal silicon PV module (STC: AM 1.5 G, +25 ^{0}C, 1000 W/m^2)

Electrical Parameters	Value
Maximum power point (P_{MPP})	180 W
Module current in the maximum power point and STC conditions (I_{MPP})	7.60 A
Short circuit current under test condition (I_{sc})	8.37 A
Nominal temperature according to STC (T_N)	25 ^{0}C
Temperature coefficient of the short circuit current (TC_I)	+0.053 %/K
Temperature coefficient of the open circuit voltage (TC_V)	-0.104 V/K
Open voltage at 25 ^{0}C and low solar irradiance ($V_{\min}$)	27 V
Open voltage at 25 ^{0}C and low solar irradiance ($V_{\max}$)	30 V
Open voltage of an unload module (V_{oc})	30 V
Low solar irradiance ($\alpha_{\min}$)	200 W/m^2
High solar irradiance ($\alpha_{\max}$)	1000 W/m^2

3. Results and Discussion

3.1. Validation of the Mathematical Modeling Using Genetic Algorithm

To validate the mathematical modeling of PV module characteristics using GA, the data sheet of PV module as shown in Table 1 was simulated for solar irradiance of 600 W/m^2, 800 W/m^2 , 1000 W/m^2, and constant temperature of 25 ^{0}C. The simulation results of current-voltage and power-voltage curve were compared to the data sheet. The curves are shown in Figure 1 to 3.

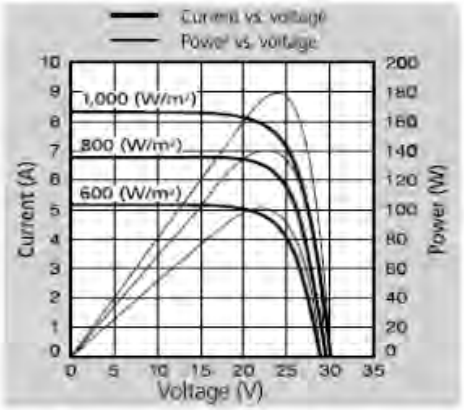

Figure 1. Current-voltage and power-voltage curve of PV module from data sheet

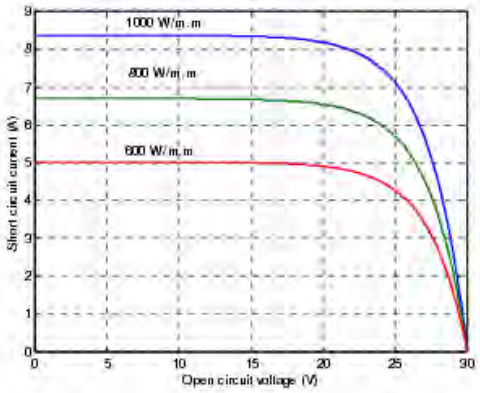

Figure 2. Current-voltage curve of PV module from simulation

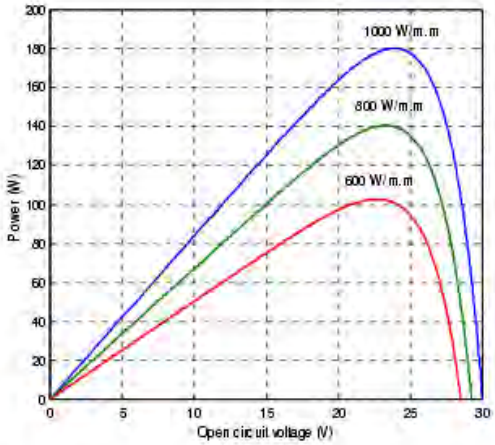

Figure 3. Power -voltage curve of PV module from simulation

The comparison of simulation results with data sheet of current-voltage and power-voltage curve in Figure1 to 3 illustrates a good correlation. Using GA, under constant temperature of 25 ^{0}C and solar irradiance of 600 W/m^2, 800 W/m^2 , 1000 W/m^2 , the short circuit current are 5.02 A, 6.70 A, 8.37 A, respectively, and the maximum power are 102.71 W, 140.56 W, 180 W, respectively. The short circuit at 600 W/m^2 in Figure 1 is 5.2 A, 3.5% higher than in Figure 2.

GA is used to find the short circuit , the open circuit voltage and the maximum power of the PV module, the equation (1) to (4) as object function. Giving a value of solar irradiance and temperature , number of generation and population of GA, the short circuit current, the open circuit voltage and the maximum power of the PV module will be appeared by the GA.

Figure 4 shows the short circuit current using GA under solar irradiance of 600 W/m^2 and temperature of 25 ^{0}C. In the running test of the program, the number of generation and population are 100 and 10, respectively. When the number of generation near 2, the GA has shown an optimum value of short circuit current, it is caused the short circuit current reached when the open circuit voltage equals zero.

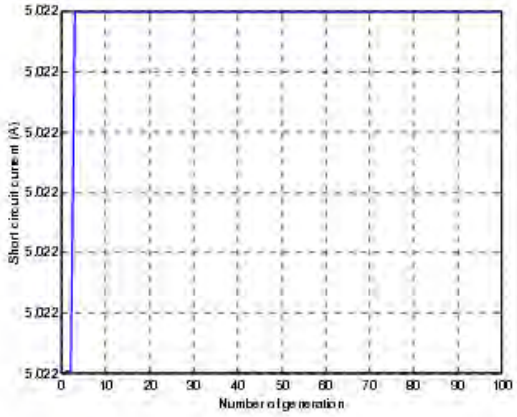

Figure 4. Short circuit current using GA under solar irradiance of 600 W/m^2 and temperature of 25 ^{0}C

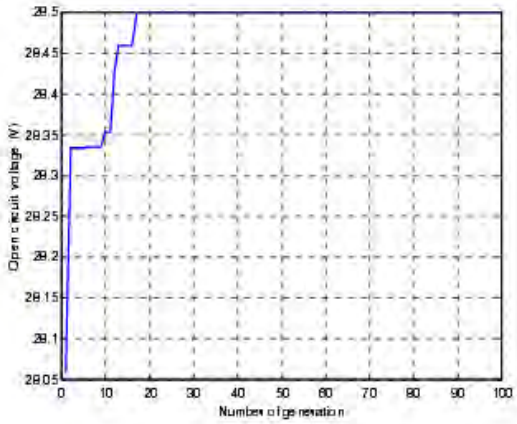

Figure 5. Open circuit voltage using GAunder solar irradiance of 600 W/m^2 and temperature of 25 ^{0}C

Figure 5 shows that the open circuit voltage using GA under of solar irradiance of 600 W/m^2 and temperature of 25 ^{0}C. When the number of generation around 17, the GA shown an optimum value of open circuit voltage, exactly 28.5 V.

Way of Figure 4 and 5 were used to get the short circuit current and the open circuit voltage of the PV module under constant temperature of 25 ^{0}C and different solar irradiance. Their results are shown in Figure 7 and 8.

The comparison of simulation results with data sheet of the short circuit current and the open circuit voltage of the PV module in Figure 6 to 8 illustrates a good correlation. Under constant temperature and different solar irradiance, if the solarr irradiance increase the short circuit current and the open circuit voltage of the PV module will increase.

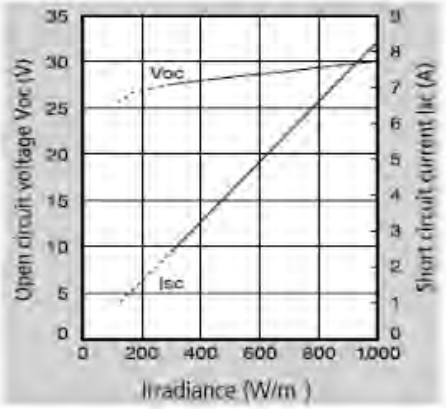

Figure 6. Short circuit currnt and open circuit voltage under constant temperature of 25 ^{0}C and different solar irradiance from data sheet

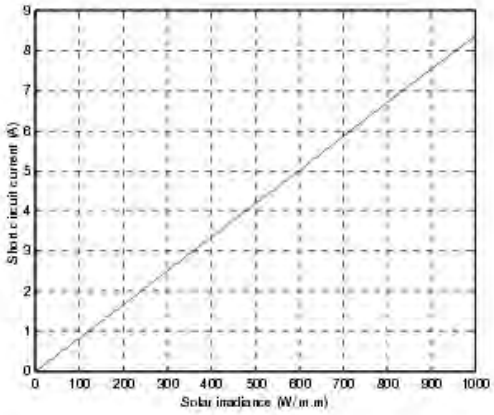

Figure 7. Short circuit current using GA voltage under constant temperature of 25 ^{0}C and different solar irradiance

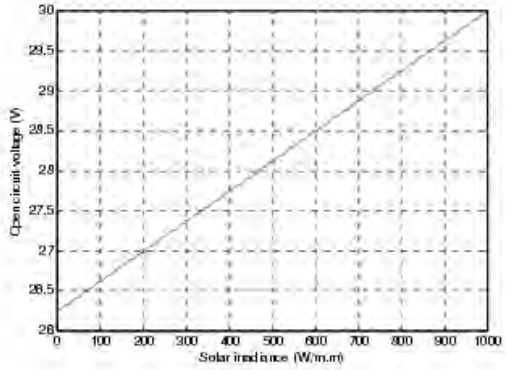

Figure 8. Open circuit voltage using GA under constant temperature of 25 ^{0}C and different solar irradiance

The simulation result of the module voltage in the maximum power point V_{MPP} and the open circuit voltage V_{oc} using GA and reference [6] are also compared as shown in Figure 10.

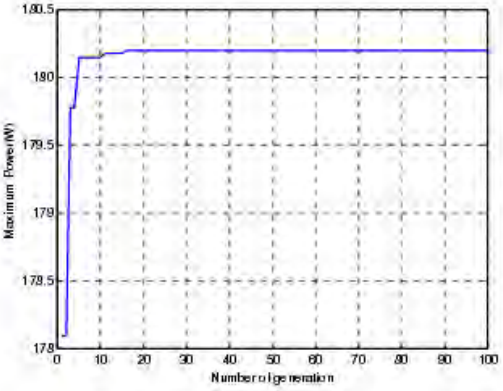

Figure 9. Maximu power of PV module using GA under solar irradiance of 1000 W/m^2 and temperature of 25 ^{0}C

Figure 9 shows that the maximum power of PV module using GA under solar irradiance of 1000 W/m^2 and temperature of 25 ^{0}C. In the running test of the program, the number of generation and population are 100 and 10, respectively. When the number of generation is around 16, the GA has shown an optimum value of the maximum power and maximum power point voltage, exactly 180 W and 23.9 V, respectively. This way is used to find the maximum power point and open circuit voltage as shown in Figure 10 under different temperature and solar irradiance.

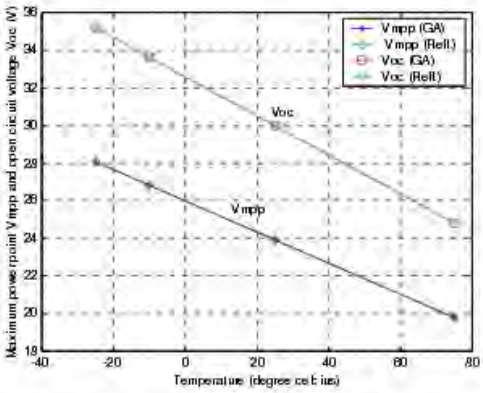

Figure 10. Maximum power point V_{MPP} and open circuit voltage V_{oc} of PV module using GA and reference [6]

The comparison of simulation results with reference [6] of the maximum power point and open circuit voltage in Figure 10 illustrates a good correlation. Using GA, under constant temperature of 25 ^{0}C and different solar irradiance produce same value of the maximum power point and open circuit voltage with reference [6].

3.2. Solar irradiance effect

The solar irradiance effect on electrical characteristics of PV module are simulated under solar irradiance of 600 W/m^2, 800 W/m^2, 1000 W/m^2 and constant temperature of 25 ^{0}C. The current-voltage and power-voltage curve of PV module are shown in Figure 2 and 3, respectively. Figure 2 shows that under constant temperature the value of the open circuit voltage scales logarithmically with the short circuit current which, in turn scales linearly with the solar irradiance resulting in a logarithmic dependence of the open circuit voltage with the solar irradiance. The solar irradiance effect on the electrical characteristics of PV module is much larger in the short circuit current than

in the open circuit voltage. The value of the short circuit current and the open circuit voltage of each the solar irradiance can be seen in Table 2.

The Figure 3 shows that under constant temperature, if the solar irradiance increase cause the maximum power of PV module will increase. The value of the PV module maximum power of each the solar irradiance can be seen in Table 2.

Table 2 shows that under constant temperature, if the solar irradiance increase cause the electrical characteristics of PV module (short circuit current, open circuit voltage, maximum power, and efficiency) will increase, the fill factor is fulfilled what discussed by [11].

Table 2. The PV module characteristics under solar irradiance of 600 W/m^2, 800 W/m^2, 1000 W/m^2 and constant temperature of 25 ^{0}C

Electrical Characteristics	Solar irradiance (W/m^2)		
	600	**800**	**1000**
I_{sc} (A)	5.02	6.70	8.37
V_{oc} (V)	28.5	29.25	30
P_{max} (W)	102.71	140.56	180
FF	0.72	0.72	0.72
η (%)	57.06	78.09	100

3.3. 3-dimensional diagram as function of both solar irradiance and temperature

The electrical characteristics of PV module are depicted as function of both solar irradiance and temperature in 3-dimensional diagrams shown in Figure 11 to 12.

Figure 11 shows that the short circuit current of PV module as function of both solar irradiance and temperature. The figure shows that if the solar irradiance is constant and the temperature increase will cause the short circuit current increase, if the temperature constant and solar irradiance increase will cause the short circuit current increase.

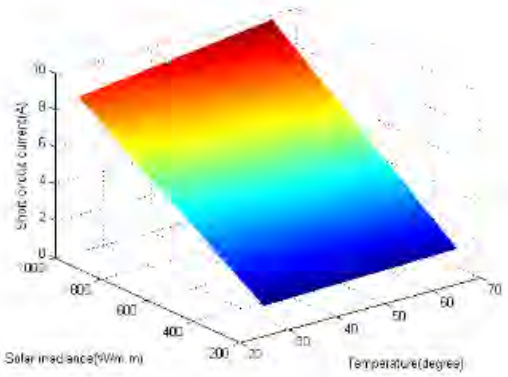

Figure 11. PV module short circuit current as function of both solar irradiance and temperature

Figure 12 shows that the open circuit voltage of PV module as function of both solar irradiance and temperature. The figure shows that if the solar irradiance is constant and the temperature increase will cause the open circuit voltage decrease, if the temperature constant and solar irradiance increase will cause the open circuit voltage increase.

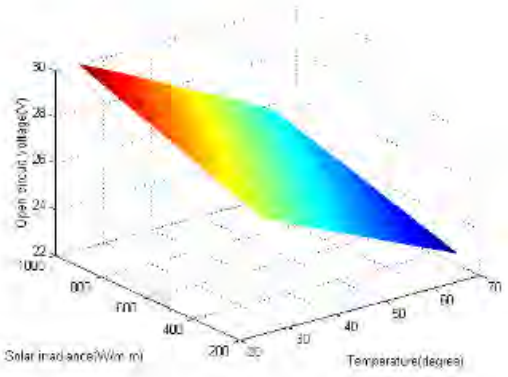

Figure 12. PV module open circuit voltage as function of both solar irradiance and temperature

Conclusion

The genetic algorithm can be used to solve optimization of PV module electrical characteristics. The electrical characteristics of PV module are dependent on solar irradiance and temperature. If the solar irradiance is constant and although the temperature increase will cause the short circuit current still constant, if the solar irradiance is constant and the temperature increase will cause the open circuit voltage, maximum power and efficiency decrease, if the temperature constant and solar irradiance increase will cause the short circuit current, open circuit voltage, maximum power and efficiency increase.

References

[1] G. Cook, L. Billman, and R. Adcock, " Photovoltaic Fundamental", DOE/Solar Energy Research Institute Report No. DE91015001, 1995.

[2] H.M. El-Zayyat, M. Mahmoud, " Photovoltaic Power Generators for Radio Communication System in Jordan", IEE proceedings, Vol. 135, Pt.C, No.5, 1988.

[3] M.J. Wu, E.J. Timpson and S.E. Watkins," Temperature Consideration in Solar Arrays", IEEE Explorer, 2004.

[4] J.I. Rosell, M. Ibanez," Modelling power output in Photovoltaic Modules for Outdoor Operating Conditions", Energy Conversion & Management, 2005, pp2424-2430.

[5] I. riedel, V. Dyakonov, J. Paris, L. Lutsen, D. Vanderzande, J.C. Hummelen," Current-Voltage Characteristics of Polymer-Fullerene Solar Cells", IEEE Explorer, 2002, pp. 1322-1325.

[6] B. Ulrick, " A Simple Model of Photovoltaic Module Electric Characteristics", IEEE Explore.

[7] G. Mitsuo, C. Runwei, " Genetic Algorithms & Engineering Design", John Wiley & Sons, INC.

[8] L. Jeremy, G. Stefan, P. Damien, C. Maurizio, G. Marcelo and M. Abdelatif, " Optimal design Analysis of A Stand Alone Photovoltaic Hybrid System", IEE Explore.

[9] http://www.energymatters.com.au/images/sharp/Sharp-NUS0E3E.pdf

[10] L. Castaner, S. Silvestre," Modelling Photovoltaic Systems Using PSpice", John Wiley & Sons, LTD.

[11] M. Irwanto, I. Daut, M. Sembiring," Electrical Characteristics of Poly-Crystal Silicon Photovoltaic Module Type 50(17) P800x541, Engineering Postgraduate Conference, 2009.

http://103.86.130.60/handle/123456789/21231

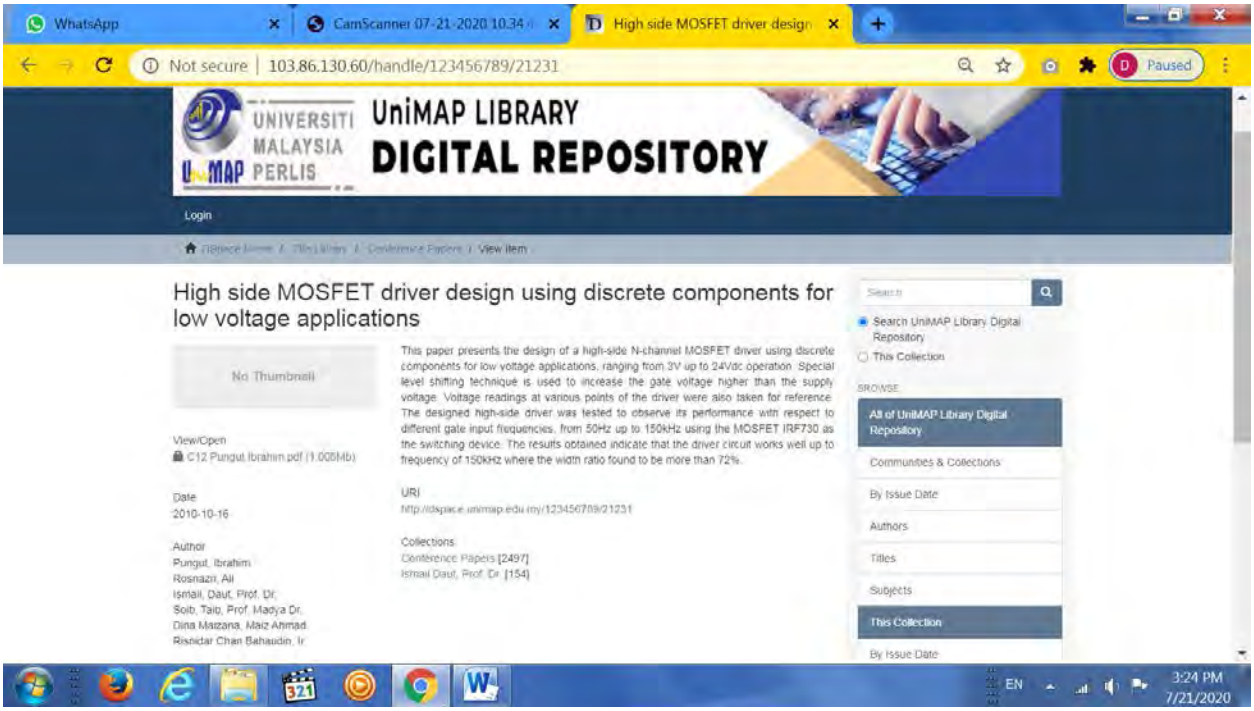

Proceedings of the International Postgraduate Conference on Engineering (IPCE 2010)
16 - 17 October 2010, Perlis, Malaysia

High Side MOSFET Driver Design Using Discrete Components for Low Voltage Applications

Pungut Ibrahim[1], Rosnazri Ali[1], Ismail Daut[1], Soib Taib[2], Dina M.M. Ahmad[1], Risnidar C.B[1]

[1]*School of Electrical Systems Engineering,*
Universiti Malaysia Perlis.
E-mail: pungut@unimap.edu.my

[2] *School of Electrical & Electronic Engineering,*
Universiti Sains Malaysia.
E-mail: soibtaib@eng.usm.my

Abstract

This paper presents the design of a high-side N-channel MOSFET driver using discrete components for low voltage applications, ranging from 3V up to 24Vdc operation. Special level shifting technique is used to increase the gate voltage higher than the supply voltage. Voltage readings at various points of the driver were also taken for reference. The designed high-side driver was tested to observe its performance with respect to different gate input frequencies, from 50Hz up to 150kHz using the MOSFET IRF730 as the switching device. The results obtained indicate that the driver circuit works well up to frequency of 150kHz where the width ratio found to be more than 72%.

1. Introduction

It is a common problem in inverter design when a MOSFET (Metal Oxide Semiconductor Field-Effect Transistor) is connected between the load and $+V_{CC}$ of the supply, especially in H-bridge inverter. The high-side MOSFET will not simply operated just by applying the gate voltage (V_{GS}) between 10V to 20V as recommended but a suitable approach must be assigned in order to put the MOSFET into its operating mode.

Custom made ICs are also available such as AN-6076, AN-978 and LM5100A that can be used to drive the high-side MOSFET [1][2][3]. Some designers experienced difficulties in getting the ICs due to certain constrains such as no stock available, long lead time and certainly this is unacceptable to urgent tasks. There are many kinds of circuits that were designed to suit with the requirements. But most of the designs need to connect the driver to the load's terminal where this arrangement will introduces undesirable negative voltage transients into the load voltage [2]. Selection of the bootstrap capacitor for the circuit is quite critical which highly depending on the frequency of operation.

For a typical bridge inverter, it is common to choose either MOSFET or IGBT (Insulated-Gate Bipolar Transistor) as a switching device. They offer several advantages over the BJTs (Bipolar Junction Transistors), ie. very high input impedance, very high switching frequency and low switching loss. The present technology in power electronics circuit, with MOSFETs and IGBTs are preferable due to variety of voltages and currents and also easily available in the market [4].

A MOSFET is a voltage driven device with typical threshold voltage between 3V to 7V. Therefore, it is very important to ensure that the V_{GS} (gate to source voltage) of the MOSFET exceeds the minimum threshold voltage in order to turn it on. In this design, MOSFET IRF730 was used for the inverter circuit as shown in Figure 1. For optimal operation, the range of V_{GS} is in between 10V to 20V for complete turn-on of the device. Partial turn-on of the MOSFET due to lower V_{GS} may introduce higher R_{DS} (drain to source resistance) and dissipating excessive heat when current flows through it. Thus, an appropriate gate voltage must be applied to drive the MOSFET into its saturation mode during turn-on state.

ISBN 978-967-5760-03-7

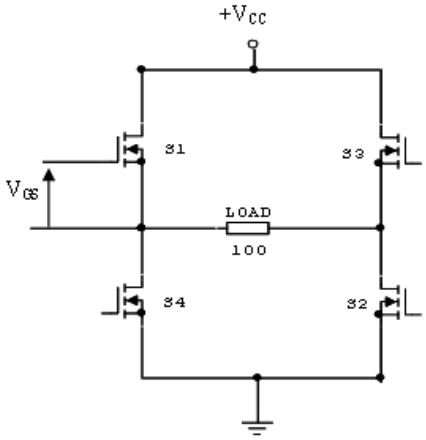

Figure 1. An H-Bridge inverter circuit

Turning on the MOSFETs S1 and S3 of the inverter can be quite tricky. At one instance, S1 needs to turn-on so that the top load is at the supply voltage ($+V_{CC}$). But the gate voltage V_{GS} has to exceed the threshold voltage, at least 7V in order to turn S1 on. Therefore by the arrangement, V_{GS} has to be at least 7V higher than the $+V_{CC}$ where this imposed to the complication due to $+V_{CC}$ is the highest available voltage we have to work with [5]. It would not be reasonable to have special higher voltage supply than +Vcc just to turn on the MOSFET. Being a high-side switch, the gate voltage is supposed to be level-shifted higher than the supply voltage when referring to the common ground. The gate must be controlled from certain logic signal which sharing the same ground [6][7][8][9].

2. Methodology

A high-side MOSFET driver circuit to drive S1 was designed and assembled as shown in Figure 2. Similarly, the same circuit can be duplicated to drive S3 for bipolar operation.

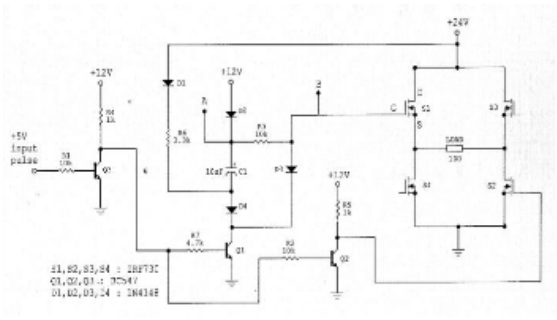

Figure 2. High-side MOSFET driver circuit

The significance of the designed driver is the level shifter components that mainly consist of C1, D1, D3 and D4. The function of the level shifter is to add-up the previously stored voltage across C1 with the +Vcc or supply voltage, as described below. This has to be achieved in order to successfully turn-on the MOSFET.

When the +5V input pulse is at low or zero volt, the transistor Q3 is turn-off, consequently turning on the transistors Q1 and Q2, resulting the MOSFET S2 to turn-off. As Q1 is on, the +12V voltage will charge-up across the capacitor C1. On the other hand, the gate terminal of S1 also connected directly to ground through Q1 and turning off S1.

Alternatively, as the input +5V input pulse is at high state, Q3 will turn-on, hence turning off Q1, Q2 and turning on MOSFET S2. As Q1 is in off state, the voltage supply of +24V appears at the collector of Q1 through the diode D1 and add-up to the voltage +12V previously stored across the capacitor C1. Therefore, the voltages at point A and B (as in Figure 2 diagram) with respect to ground would be 36V, thus triggers S1. From the data sheet of IRF730, it is specified that the typical gate threshold voltage (V_{GS}) is 3V, hence any voltage applied across that exceeding 3V will certainly turn it on.

3. Results

A constant +5V dc trigger voltage was applied to the input of the driver, with the transistors (Q1, Q2 &Q3) collector voltage of 12.17V and V_{CC} of 24.39V. Voltage measurements were taken at the specified points referring to Figure 2 circuit.

The voltage at point A = 36.56V and
the voltage at point B = 36.56V and
the threshold voltage (V_{GS}) = 3.60V

When there was no +5V dc trigger voltage to the input,

The voltage at point A = 11.58V and
the voltage at point B =0.625V
the threshold voltage (V_{GS}) = 0.0V

The frequency response of the driver was tested as shown in Figure 3 until Figure 11. CH1 represents switching signal voltage at input side of the driver circuit and CH2 indicates the voltage across the 100 Ohm load resistor.

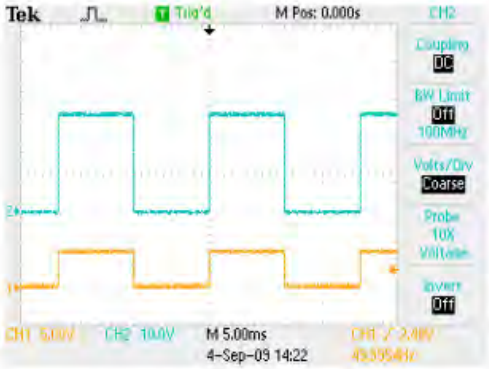

Figure 3. 50Hz input switching signal

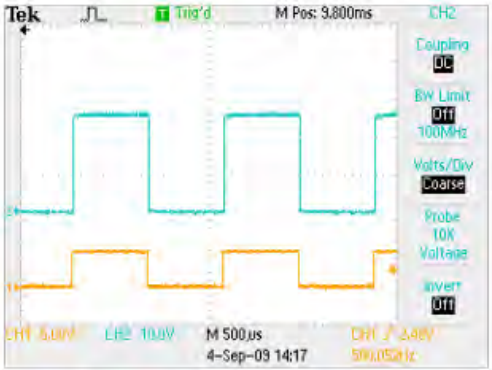

Figure 4. 500Hz input switching signal

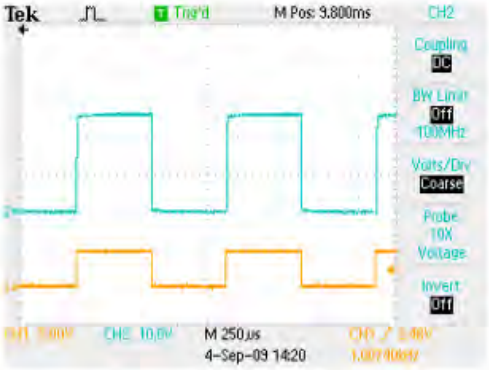

Figure 5. 1kHz input switching signal

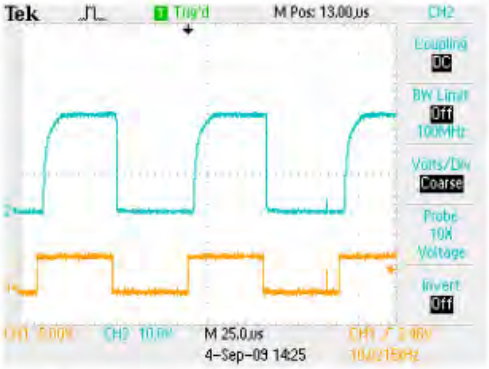

Figure 6. 10kHz input switching signal

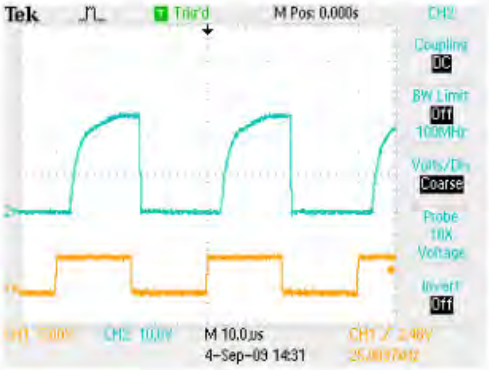

Figure 7. 25kHz input switching signal

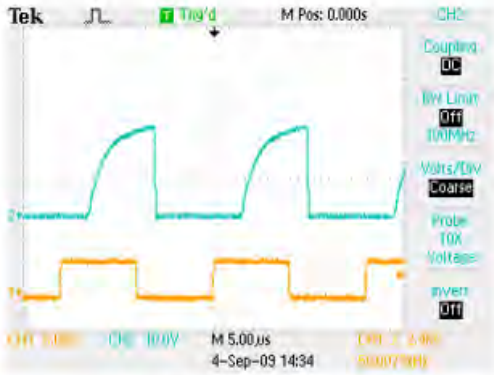

Figure 8. 50kHz input switching signal

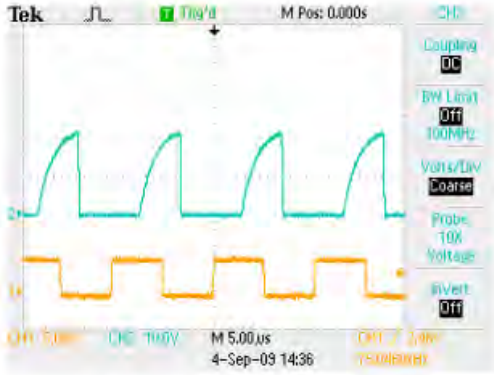

Figure 9. 75kHz input switching signal

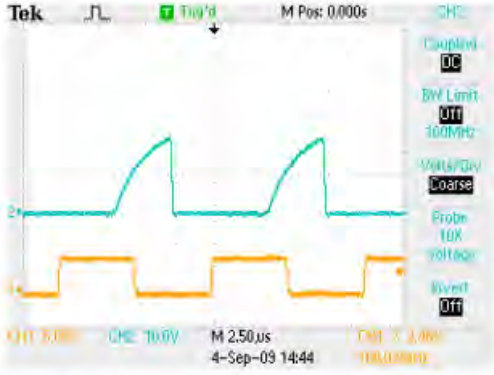

Figure 10. 100kHz input switching signal

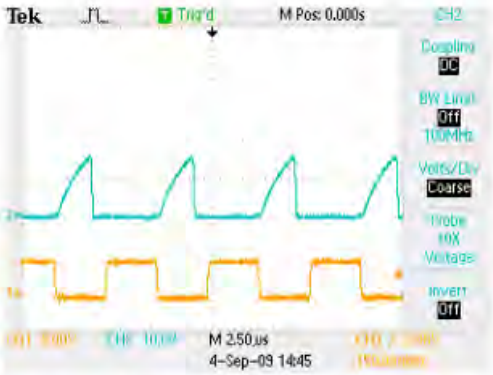

Figure 11. 150kHz input switching signal

Table 1 shows the summary of the results obtained for the input and output widths and the peak voltage output with respect to different input frequencies. The percentage width ratio is calculated from the output width divided by input width.

Table 1. Summary of the results

Freq. (kHz)	Input Width (μs)	Output Width (μs)	% Width Ratio	Peak Voltage Output (V)
0.05	10000.00	10000.00	100.0	26.4
0.5	1000.00	1000.00	100.0	26.4
1	500.00	500.00	100.0	26.4
10	50.00	50.00	100.0	26.4
25	20.00	18.80	94.0	26.0
50	10.00	8.60	86.0	23.6
75	6.60	5.20	78.8	21.6
100	5.00	3.90	78.0	20.0
150	3.30	2.40	72.7	16.0

The performances of the designed MOSFET driver can be observed from the trends that are shown in Figure 12 and 13.

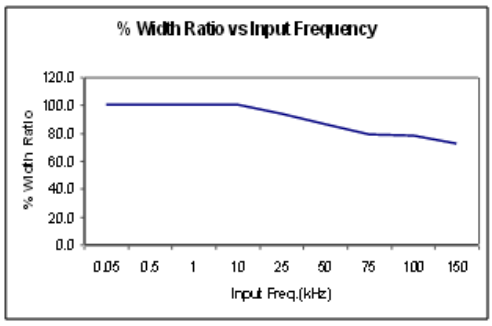

Figure 12. % Width Ratio vs Input Frequency

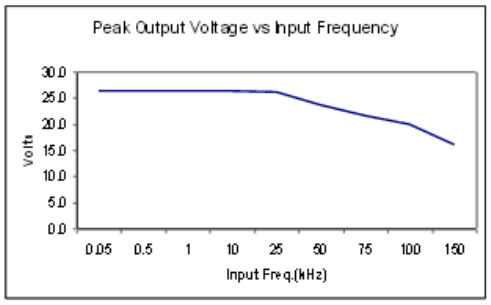

Figure 13. Peak Output Voltage vs Input Frequency

4. Discussion

The results determined the driver circuit performance in response to several input driving frequencies.

At lower frequencies from 50Hz to 1kHz, the voltages at point A (as in Figure 2 diagram) and across the load resistor were observed that the original square-wave had the shape as the input. As the frequencies increased from 10kHz to 50kHz, the waveform of the voltages began to change in shape due to the effect of capacitor C1. Referring at 50kHz waveforms, the output voltage across the load resistor shows a slow rise of the peak amplitude, with the capacitor's voltage (at point A) encounters slight distortion.

The frequency response of the output voltage could be improved by changing the capacitance C1 to a lower value when dealing with higher frequencies input. At point A (CH2), it is noted that the voltage level is shifted from 12V to 32.4V. This happen when capacitor C1 storing the 12V and add-up with the 24V (supply) into the next pulse, which is enough to turn-on the MOSFET S1.

As indicated in Figure 12, the percentage width ratio trend between output and input waveforms starts to slope-down below 90% as the input frequencies exceeding 25kHz and at 150kHz the width ratio falls to 72.7%. Similarly, for the peak output voltage shown in Figure 13, the voltage starts to drop below than 26V as the input frequencies increased beyond 25kHz.

For H-bridge inverter the MOSFETs or IGBTs will operate satisfactorily for operating frequency, below than 25kHz. This could be suitable for critical and sensitive loads. For non-critical loads, the frequency operation could be different.

5. Conclusion

The objective of designing high-side MOSFET driver is achieved using commonly available discrete components. The driver circuit generally can be used to drive the high-side MOSFETs of a bridge inverter to frequencies beyond 25kHz and is concluded the best recommended operational amplitude for the system is up to 100kHz for width ratio to be under 20% of discrepancy.

6. References

[1] National Semiconductor Data Sheet LM5100A/B/C, June 9, 2009.

[2] Fairchild Application Note AN-6076 : Design and Application Guide of Bootstrap Circuit for High Voltage Gate Drive IC.

[3] International Rectifier Application Note AN978 : HV Floating MOS-Gate Driver ICs.

[4] MH Rashid, "Power Electronics Circuits, Devices and Applications", 3rd Ed.,Prentice-Hall, 2003, pp 761~789.

[5] SK Mazalan, "Design, Construct and Evaluate a Step-up Inverter using High Frequency Switching Technique", UG Thesis, Electrical Eng. Department 2008, Universiti Malaysia Perlis. pp 21~23.

[6] M.Kong; W.Yan; W. Li, "Design of a synchronous-rectified buck bootstrap MOSFET driver for voltage regulator module," *ASIC, 2007. ASICON '07. 7th International Conference on* , vol., no., pp.974-977, IEEE.

[7] Swart, A.J.; Pienaar, H.C.V.; Case, M.J., "A radio frequency MOSFET driver," *AFRICON, 2004. 7th*

AFRICON Conference in Africa , vol.1, no., pp.543-546 Vol.1, 17-17 Sept. 2004, IEEE.

[8] Pathak, A.D.; Ochi, S., "Unique MOSFET/IGBT drivers and their applications in future power electronic systems," *Power Electronics and Drive Systems, 2003. PEDS 2003. The Fifth International Conference on* , vol.1, no., pp. 85-88 Vol.1, 17-20 Nov. 2003, IEEE.

[9] Abbate, C.; Busatto, G.; Iannuzzo, F.; Fratelli, L., "Experimental characterisation of high efficiency resonant gate driver circuit," *Power Electronics and Applications, 2007 European Conference on* , vol., no., pp.1-8, 2-5 Sept. 2007, IEEE.

http://103.86.130.60/handle/123456789/21219

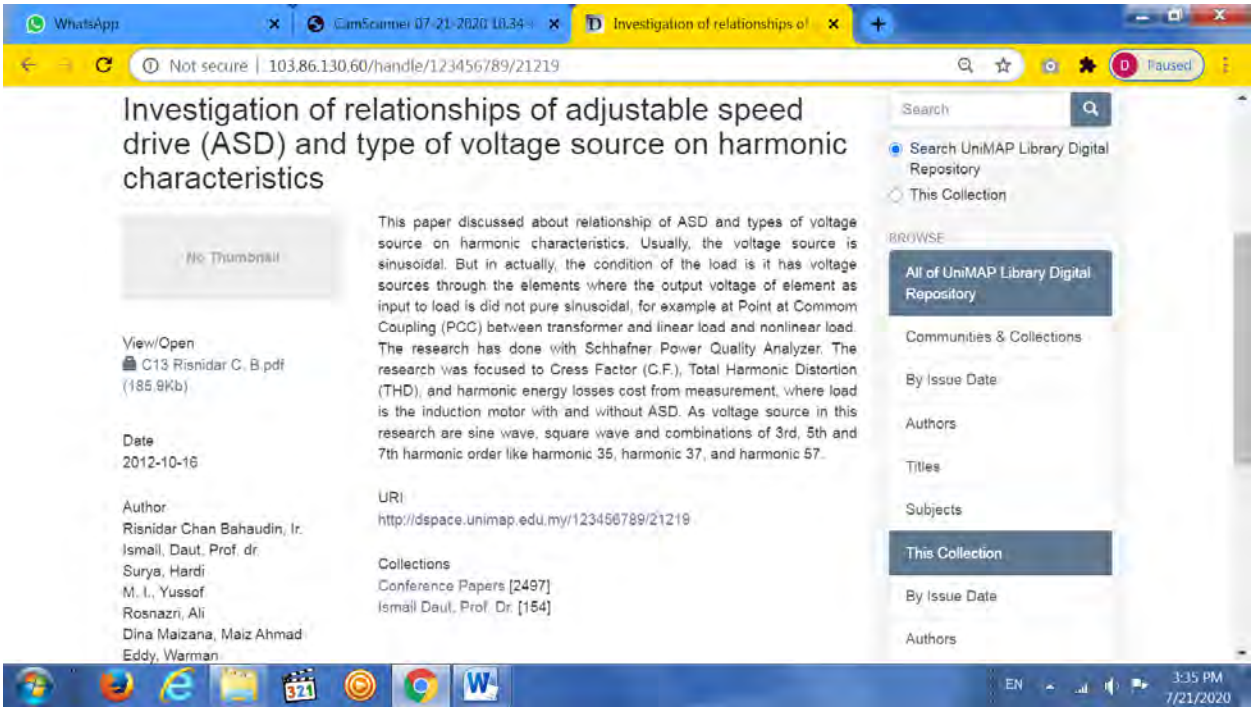

Proceedings of the International Postgraduate Conference on Engineering (IPCE 2010)
16 - 17 October 2010, Perlis, Malaysia

Investigation of Relationships of Adjustable Speed Drive (ASD) and Type of Voltage Source on Harmonic Characteristics

[1]Risnidar C.B, [2]Ismail Daut, [1]Surya hardi, [1]M.I. Yussof, [1]Rosnazri Ali,
[1]Dina M.M. Ahmad, [3]Eddy Warman, [3]Masykur
[1]Ph.D student UniMAP
[2]Supervisor Ph.D student UniMAP
Electrical Engineering Department, University Malaysia Perlis (UniMAP), Kangar, Malaysia
[3]Master Student USU
Electrical Engineering Department, Universitas Sumatera Utara, Medan, Indonesia.
Email: risnidar@unimap.edu.my

Abstract

This paper discussed about relationship of ASD and types of voltage source on harmonic characteristics. Usually, the voltage source is sinusoidal. But in actually, the condition of the load is it has voltage sources through the elements where the output voltage of element as input to load is did not pure sinusoidal, for example at Point at Commom Coupling (PCC) between transformer and linear load and nonlinear load. The research has done with Schhafner Power Quality Analyzer. The research was focused to Cress Factor (C.F.), Total Harmonic Distortion (THD), and harmonic energy losses cost from measurement, where load is the induction motor with and without ASD. As voltage source in this research are sine wave, square wave and combinations of 3rd, 5th and 7th harmonic order like harmonic 35, harmonic 37, and harmonic 57.

Keywords—type of voltage source, energy losses cost, harmonic, THD.

1. Introduction

Reason in this research discussing the kinds of voltage sources used to serve the load, such as sine wave, square wave and the combination of the harmonics order, so necessary to discuss about Fourier series, because to analyze the harmonics, applied the Fourier series is appropriate. Actually, Fourier series is a periodic function and can be written as sums of infinitely many sine and cosine functions of different frequencies R.J. Beerends et al (2003) [1], often expressed in terms of the angular frequency. Harmonic waveform distortion is one of the most important issues today. Discuss about investigation of harmonic effect due to harmonic types of voltage source, where the voltage sources are a few types of harmonic waveform. This case is as a part of system, where if a Point of Common Coupling (PCC) of one component nonlinear load has supplied with another nonlinear load. In this research, the load is Induction Motor was supplied with Sine waveform, Harmonic 3rd, 5th, and 7th combination waveform.

The presence of harmonic distortion in the applied voltage to a motor will both increase electrical losses and decrease efficiency. These losses will increase motor temperature, resulting in even further losses These currents passing through the system impedance cause voltage drops for each individual harmonic, resulting in distortion of the voltage's waveform. The effect of harmonic distortion of the voltage waveform due to impacts motor performance as p.f. IHD and THD for current and voltage, and energy losses due to harmonic. [2][3][4].

$$p.f. = \frac{P}{S} = \frac{kW}{kVA} = \cos\varphi \qquad (1$$

$$S = \sqrt{P^2 + Q^2} \qquad (2)$$

$$kVA = \sqrt{kW^2 + kVAR^2 + kVAR_H^2} \qquad (3)$$

True Power factor = (Displacement p.f) x (Distortion p.f.)

ISBN 978-967-5760-03-7

The others characteristic of harmonic are:

The values of V_{rms} I_{rms}, Power (P), were calculated directly from the harmonic components obtained with a Fast Fourier Transform of the sampled data of the voltage and current waveforms of the Induction Motor under tests. These quantities were calculated as:[3][4][5][6]

$$V_{rms} = \sqrt{\sum_{h=1}^{\infty} V_h^2} \text{ and } I_{rms} = \sqrt{\sum_{h=1}^{\infty} I_h^2} \qquad (4)$$

$$P = \sum_{h=1}^{\infty} V_h I_h \cos\varphi_h \text{ and } S = V_{rms} I_{rms} \qquad (5)$$

where V_h, I_h φ_h are magnitudes and phase shift of the voltage and current, h order harmonic.
The factor that measures the distortion in the non sinusoidal wave is Total Harmonic Distortion (THD) where this factor is defined for both voltage and current as below:

$$THD_I = \frac{\sqrt{\sum_{h=2}^{\infty} I_h^2}}{I_1} \text{ and } THD_V = \frac{\sqrt{\sum_{h=2}^{\infty} V_h^2}}{V_1} \qquad (6)$$

2. Methodology

From the measurement of induction motor with Shaffner, where the voltage source to load is varieties are: sinusoidal, and a few harmonics waveforms. And the load is three phase induction motor. To study the effect of voltage source type of harmonic to served load, the measurement of induction motor with Shaffner, where the voltage source to load is varieties are: sinusoidal, and a few harmonics waveform are done . Because at any PCC in power system, the load maybe find source did not pure sinusoidal, for example from secondary of transformer. The main characteristic of harmonics are Individual Harmonic Distortion (IHD) for 3rd ,5th and 7th, Total Harmonic Distortion (THD) for voltage and current, Power losses due to harmonics, power factor, Cress factor for each harmonics, I_{rms}, V_{rms}. The measurements are done with voltage sources variable from 160 V until 240 V.

The type of voltage source from combination of harmonic order 3rd, 5th and 7th are as Figure 1 below.

The Induction motor specifications are: 3 phase, 1.5 Hp, 50 Hz, 1370 rpm, 4 poles. The measurements have done without ASD and with ASD.

Figure1. Type of voltage source from 3rd, 5th and 7th Harmonic order combinations

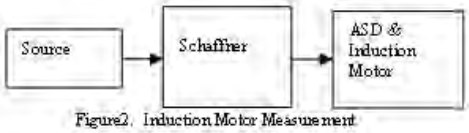

Figure2. Induction Motor Measurement

3. Data and result

Data and result base direct measurements to induction motor 3 phase, 1.5 Hp, 50 Hz, 1370 rpm, 4 poles are as follow:

Table 1. Type of voltage source Vs, power active, Apparent Power, p.f and speed

V.Source	P(kW)	S(kVA)	p.f.	C.F.	Speed(rpm)
Harm35	0.0348	0.1816	0.302	1.718	1779
Harm37	0.0344	0.1782	0.296	1.596	1551
Harm57	0.0358	0.184	0.304	1.782	1579
Sine	0.0362	0.1816	0.316	1.528	1577
Square	0.0366	0.1696	0.32	2.292	1484

Table 2. The condition Irms with and without ASD

No	Vsource	ASD	Without ASD	Delta Irms
1	Harm35	0.44	1.88	1.43
2	Harm37	0.58	1.84	1.27
3	Harm57	0.87	1.91	1.04
4	Sine	0.53	1.88	1.35

Table 3. The condition real power P with and without ASD

No	V source	ASD	Without ASD	Delta P
1	Harm35	0.03	0.07	0.04
2	Harm37	0.04	0.07	0.03
3	Harm57	0.05	0.07	0.02
4	Sine	0.04	0.07	0.03
5	Square	0.03	0.07	0.03

Table 4. The condition apparent power S with and without ASD

No	V source	ASD	Without ASD	Delta S
1	Harm35	0.11	0.45	0.34
2	Harm37	0.14	0.44	0.30
3	Harm57	0.21	0.46	0.25
4	Sine	0.13	0.45	0.33
5	Square	0.12	0.39	0.27

Table 5. The condition power factor p.f. with and without ASD

No	Vsource	ASD	Without ASD	Delta p.f.
1.00	Harm35	0.28	0.16	0.12
2.00	Harm37	0.30	0.16	0.14
3.00	Harm57	0.25	0.16	0.09
4.00	Sine	0.29	0.16	0.13
5.00	Square	0.29	0.18	0.11

Table 6. The condition 3rd V with and without ASD

No	V source	ASD	Without ASD	Delta 3rd V
1	Harm35	10.01	0.21	9.80
2	Harm37	10.02	10.04	-0.02
3	Harm57	0.24	0.26	-0.02
4	Sine	0.22	0.22	0.00
5	Square	33.39	33.41	-0.02

Table 7. The condition 5th V with and without ASD

No	Vsource	ASD	Without ASD	Delta 5thV
1	Harm35	4.97	0.09	4.88
2	Harm37	0.15	0.12	0.03
3	Harm57	10.04	10.01	0.03
4	Sine	0.08	0.04	0.04
5	Square	19.92	19.88	0.04

Table 8. The condition 7th V with and without ASD

No	Vsource	ASD	Without ASD	Delta 7th V
1	Harm35	0.06	9.92	-9.86
2	Harm37	4.95	4.94	0.01
3	Harm57	4.97	4.95	0.02
4	Sine	0.02	0.01	0.01
5	Square	13.95	13.88	0.07

Table 9. The condition THD_V with and without ASD

No	V source	ASD	Without ASD	Delta THDV
1	Harm35	11.15	9.89	1.26
2	Harm37	11.11	11.13	-0.02
3	Harm57	11.15	11.1	0.05
4	Sine	0.27	0.23	0.04
5	Square	41.11	41.12	-0.01

Table 10. The condition 3rd I with and without ASD

No	V source	ASD	Without ASD	Delta 3rd I
1	Harm35	83.64	0.54	83.10
2	Harm37	75.26	1.14	74.12
3	Harm57	96.28	0.43	95.85
6	Sine	95.67	0.48	95.19
7	Square	63.54	2.66	60.88

Table 11. The condition 5th I with and without ASD

No	Vsource	ASD	Without ASD	Delta 5th I
1	Harm35	86.67	2.21	84.46
2	Harm37	95.36	1.89	93.47
3	Harm57	94.42	22.72	71.70
4	Sine	94.23	1.54	92.69
5	Square	94.27	46.36	47.91

Table 12. The condition 7th I with and without ASD

No	V source	ASD	Without ASD	Delta 7th I
1	Harm35	80.61	13.48	67.13
2	Harm37	95.36	6.11	89.25
3	Harm57	90.33	7.38	82.95
4	Sine	91.35	1.22	90.13
5	Square	90.1	23.25	66.85

Table 13. The condition THD_I with and without ASD

No	V source	ASD	Without ASD	Delta THD I
1	Harm35	91.92	13.75	78.17
2	Harm37	92.87	6.65	86.22
3	Harm57	93.33	23.01	70.32
4	Sine	91.2	2.23	88.97
5	Square		47.25	-47.25

The waveform of voltages and currents for type of voltage source are as follow;

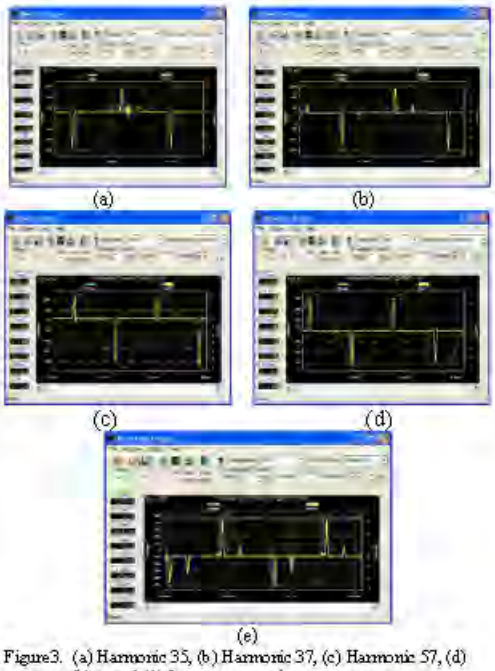

Figure3. (a) Harmonic 35, (b) Harmonic 37, (c) Harmonic 57, (d) Sine and (d) Square wave voltage source

4. Analysis

From experiment data and results the analysis for harmonic characteristics are as follow:

4.1. Real power (P) in kW

For power P, harmonic 57 is highest (0.05), but the different between with and without ASD very small (0.02) and harmonic 35 similar to square wave (0.03). For without ASD all types just the same (0.07).

4.2. Apparent power (S) in kVA

The highest apparent power is harmonic 57 (10.184) and the lowest is square (0.1696). Different between with and without ASD, harmonic 35 is highest (0.34).

4.3. Power factor (p.f.)

Power factor (p.f) for square wave without ASD is highest (0.18), while the others voltage source just the same (16). With ASD, p.f were increase and the highest is harmonic 37 (0.30) while the lowest is harmonic 57 (0.25).

4.4. 3rd Voltage harmonic

For 3rd harmonic, with ASD condition sine wave is smallest (0.22%) and constant without ASD (0.22%) while square wave is highest (33.39%). Different between with ASD and without ASD, harmonic 35 is highest (9.80%).

4.5. 5th Voltage harmonic

For 5th harmonic, with ASD condition sine wave is smallest (0.08%) while square wave is highest (19.92%). Different between with ASD and without ASD, harmonic 35 is highest (4.88%).

4.6. 7th Voltage harmonic

Sine wave is the smallest with ASD (0.02%) and without ASD (0.01%), while square wave is the biggest (13.95%) with ASD and (13.88%) without ASD, but for different between with ASD and without ASD, Harmonic 35 is the biggest (9.86%).

4.7. THD harmonic voltage

As for 7th harmonic order, sine wave is the smallest with ASD (0.27%) and without ASD (0.23%), while square wave is the biggest (41.11%) with ASD and (41.12%) without ASD, but for different between with ASD and without ASD, Harmonic 35 is the biggest (1.26%).

4.8. 3rd current harmonic

For current Individual Harmonic Distortion (IHD) 3rd order, harmonic 57 is biggest (96.28%), while the smallest is square wave (63.54%) with ASD, but without ASD, sine wave is smallest (0.48%) and square wave is biggest (2.66%).

4.9. 5th current harmonic

For current Individual Harmonic Distortion (IHD) 5th order, harmonic 37 is biggest (95.36%), while the smallest is harmonic 35 (86.67%) with ASD, but without ASD, sine wave is smallest (1.54%) and square wave is biggest (46.36%).

4.10. 7th current harmonic

For current Individual Harmonic Distortion (IHD) 7th order, harmonic 37 is biggest (95.36%), while the smallest is harmonic 35 (80.61%) with ASD, but without ASD, sine wave is smallest (1.22%) and square wave is biggest (23.25%). but for different between with and without ASD, sine wave is the biggest (90.13%).

4.11. THD current harmonic

For current Total Harmonic Distortion (THD) harmonic 57 is biggest (93.33%), while the smallest is sine wave (91.2%) with ASD, but without ASD, sine wave is smallest (2.23%) and square wave is biggest (47.25%). but for different between with and without ASD, sine wave is the biggest (88.97%).

5. Conclusion

From analyze, the conclusion are:

1. Real power and apparent power loss due to type of voltage source, harmonic 57 is biggest.
2. Without ASD, power factor (p.f) is the highest for square wave and with ASD, is highest for harmonic 37.
3. For sine wave, voltage Individual Harmonic Distortion (IHD) 3rd, 5th and 7th is the smallest, square wave is the highest and different between with and without ASD, harmonic 35 is highest. According with these, Total Harmonic Distortion (THD) is similar.
4. For condition without ASD, current Individual Harmonic Distortion (IHD) 3rd, 5th, 7th and Total harmonic Distortion (THD), sine wave is smallest and square wave is largest. But with ASD, for 3rd order, harmonic 57 is largest, 5th and 7th order harmonic 37 is largest, and smallest is harmonic 35.

6. Acknowledgement

The authors would like to express their gratitude to the Fundamental Research Grant Scheme (FRGS), School of Electrical System Engineering of Universiti Malaysia Perlis (UniMAP) and Power Electronics and Electrical Machine Design Research Cluster for the supply of research facility respectively.

7. References

[1]. R. J. Beerends, H. G. Morshe, J. C. van den Berg and E. M. van de Vrie, "*Fourier and Laplace Transforms*", Translated from Dutch by R.. J. Beerends, Cambridge University Press, 2003.

[2]. Peter Bechard, *"Fault ZoneAnalysis POWER QUALITY"*, The 2004 Motor Reliability Technical Conference, PdMA Corporation.

[3]. Barry W. Kennedy, POWER QUALITY PRIMER, McGraw-Hill, Singapore, 2000

[4]. Francisco C. De La Rosa, "Harmonics and Power Systems", Taylor & Frencis, CRC, Boca Raton, 2006.

[5]. J. Arrilaga, B.C.Smith, N.R. Watson, A.R. Wood, POWER SYSTEM HARMONIC ANALYSIS, John Wiley & Sons, Singapore, 2000

[6]. IEEE Recommended Practices and Requirements for Harmonic Control in Electrical Power Systems